HIV-1 unmasks the plasticity of innate lymphoid cells

Yetao Wang,[1] Kyle Gellatly[2], Alan Derr,[2] Smita Jaiswal,[1] Alper Kucukural,[2] Patrick McDonel,[2] Thomas Greenough,[1] JeanMarie Houghton,[3] Manuel Garber,[1,2] and Jeremy Luban[1,4,*]

[1]Program in Molecular Medicine, University of Massachusetts Medical School, 373 Plantation Street, Worcester MA 01605, USA

[2]Program in Bioinformatics and Integrative Biology, University of Massachusetts Medical School, Worcester, MA 01655, USA

[3]Department of Medicine, University of Massachusetts Medical School, 364 Plantation Street, Worcester, MA 01605, USA

[4]Department of Biochemistry and Molecular Pharmacology, University of Massachusetts Medical School, 364 Plantation Street, Worcester, Massachusetts 01605, USA

*Correspondence to Jeremy Luban: jeremy.luban@umassmed.edu

ABSTRACT

Pharmaceuticals that suppress HIV-1 viremia preserve $CD4^+$ T cells and prevent AIDS. Nonetheless, HIV-1 infected people taking these drugs have chronic inflammation attributable to persistent disruption of intestinal barrier function with increased rates of cardiovascular mortality. To better understand the etiology of this inflammation we examined the effect of HIV-1 infection on innate lymphoid cells (ILCs). These innate immune counterparts of T cells lack clonotypic antigen receptors, classify according to signature transcription factors and cytokines, and maintain homeostasis in inflamed tissues. ILCs have been defined, in part, by the IL-7Rα, CD127. Here we report that the vast majority of type 1 and 3 ILCs in human adult and placental cord blood are in fact $CD127^-$, as are colon lamina propria ILC1s and many ILC3s. Among ILCs, $CD127^-$ILC1s were the major producer of inflammatory cytokines. In contrast to $CD127^+$ILC3s, $CD127^-$ILC3s did not produce IL-22, a cytokine that maintains epithelial barrier function. In HIV-1^+ people taking antivirals that preserve $CD4^+$ T cells, $CD127^-$ILC1s and all homeostatic cytokine-producing $CD127^+$ILCs were decreased in blood and colon. Common γ-chain cytokines that are reported to be elevated in response to HIV-1 infection caused JAK3-dependent downregulation of CD127 and converted $CD127^-$ ILC1s into NK cells with heightened cytolytic activity. Consistent with the recent report that human blood $CD117^+$ILCs give rise to both ILC1s and NK cells, pseudotemporal clustering of transcriptomes from thousands of individual cells identified a developmental trajectory from $CD127^-$ILC1s to memory NK cells that was defined by WNT-transcription factor TCF7. WNT inhibition prevented the cytokine-induced transition of $CD127^-$ILC1 cells into memory NK cells. In HIV-1^+ people, effector NK cells and $TCF7^+$ memory NK cells were elevated, concomitant with reduction in $CD127^-$ ILC1s. These studies describe previously overlooked human ILC subsets that are significant in number and function, identify profound abnormalities in homeostatic ILCs that likely contribute to ongoing inflammation in HIV-1 infection despite control of viremia, provide explanation for increased memory NK cells in HIV-1 infection, and reveal functional plasticity of ILCs.

GRAPHICAL ABSTRACT

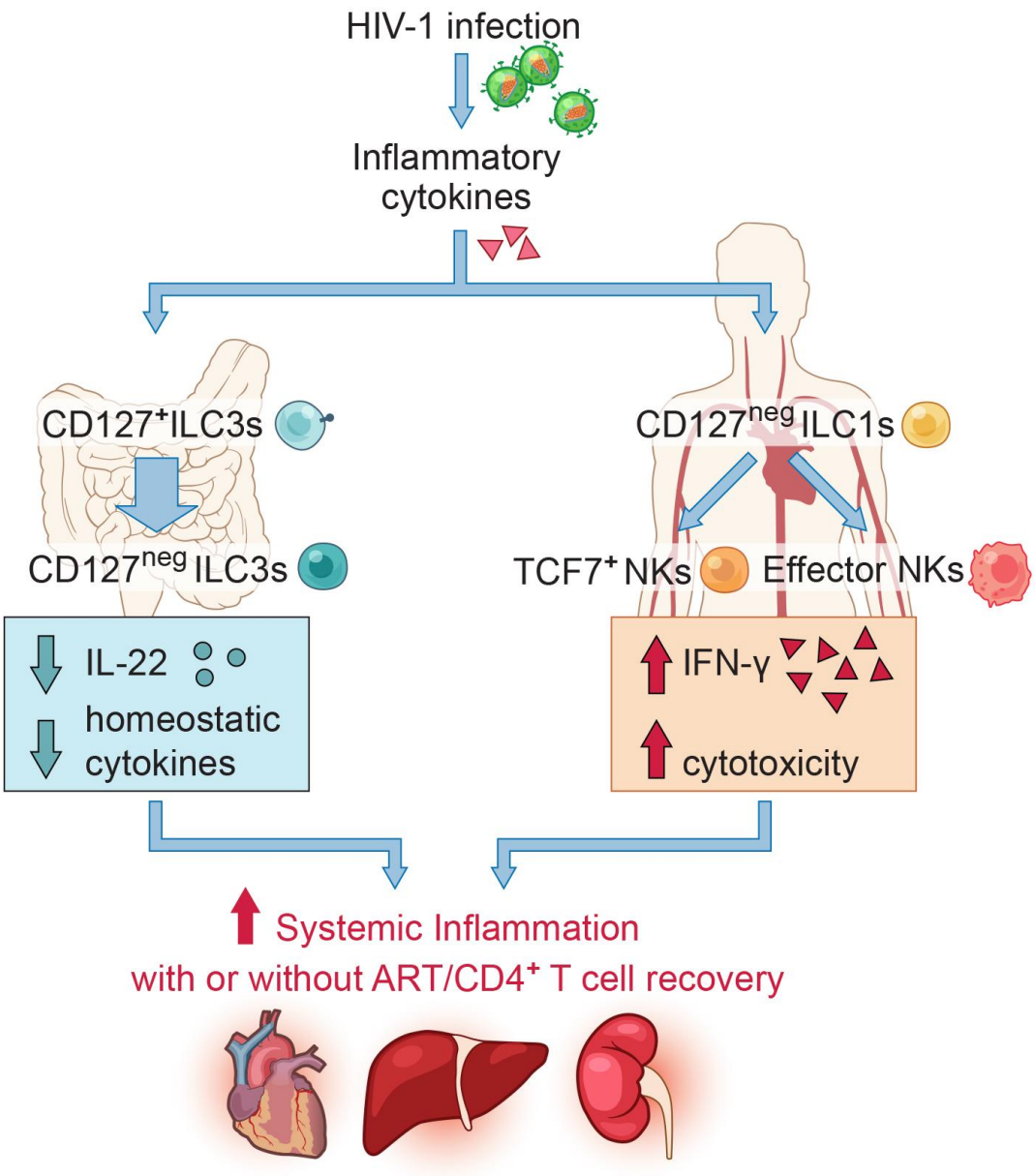

INTRODUCTION

HIV-1 infection is lifelong and no treatments yet available reliably eliminate the virus from infected people (Margolis et al., 2016). Given uninterrupted access to antiviral drug combinations that suppress HIV-1 viremia it is possible to preserve $CD4^+$ T cells and prevent progression to AIDS (Günthard et al., 2016; Taieb et al., 2017; Tucker et al., 2017). Nonetheless, infected individuals on these antiviral therapies have chronic inflammation with increased rates of cardiovascular mortality (Freiberg et al., 2013; Sinha et al., 2016). This pathology has been attributed to permanent disruption of cellular networks that maintain the integrity of the intestinal epithelium and limit the intestinal microbiome (Brenchley et al., 2006; Deeks et al., 2013; Klatt et al., 2012).

Innate lymphoid cells (ILCs) are counterparts of T cells that lack clonotypic antigen receptors or other lineage-defining cell surface markers (Hazenberg and Spits, 2014; Spits et al., 2013). Like T cells, they are classified into subsets according to the signature transcription factors that they express and the effector cytokines that they produce (Serafini et al., 2015). Among the many subsets of ILCs are natural killer (NK) cells that are capable of lysing tumor cells and virus-infected cells (Spits et al., 2016; Vivier et al., 2008). ILCs carry out a large range of biological functions, including roles in host defense against pathogens and maintenance of homeostasis in inflamed tissues (Artis and Spits, 2015; Klose and Artis, 2016; Spits et al., 2016).

ILCs have been defined as Lin^-CD127^+ cells that are divided into three main subsets - ILC1s, ILC2s, and ILC3s - based on expression of TBX21, GATA3, or RORγT, respectively (Spits et al., 2013; Walker et al., 2013). Mouse NK cells are Lin^-Tbx21^+, but, unlike ILC1s, they are $CD127^-$ and $Eomes^+$, and they develop independently of the $ID2^+$ common helper-like ILC progenitor (Klose et al., 2014). However, human NK cells and ILCs are capable of differentiating from a common Lin^-CD117^+ cell (Lim et al., 2017), and several observations challenge the use of CD127 or Eomes to distinguish ILC1s and NK cells. CD127 is not required for development of all ILC subtypes; the number of lymphoid-tissue-inducer (LTi) cells, a subset of ILC3s, is normal in the blood and spleen of $CD127^{-/-}$ or $IL\text{-}7^{-/-}$ mice (Luther et al., 2003; Schmutz et al., 2009). Eomes

is not required for the formation of NK cells, its expression can be induced in Eomes$^-$ Tbx21$^+$NK cells (Gordon et al., 2012) or repressed by TGF-β (Cortez et al., 2016). Given the uncertain significance of CD127 and EOMES, several human studies have used CD94 to distinguish NK cells from ILCs (Björklund et al., 2016; Hazenberg and Spits, 2014), and single cell RNA-Seq has shown that the transcriptional profile of CD94$^+$NKG2A$^+$NK cells is distinct from CD94$^-$/NKG2A$^-$ILC1s and other ILCs (Björklund et al., 2016).

Several observations suggest that ILCs play roles in HIV-1-associated pathology and in anti-HIV-1 immunity. Blood ILCs are irreversibly depleted by HIV-1 if antiviral therapy is not started within a few weeks of acute infection (Kløverpris et al., 2016). The contribution of ILC deficiency to HIV-1-associated chronic inflammation remains unclear since abnormalities in homeostatic colon lamina propria ILCs were not observed (Kløverpris et al., 2016). NK cells kill HIV-1-infected cells (Alter et al., 2011) and SIV-infected macaques have NK cells with apparent antigen-specific memory responses (Reeves et al., 2015). The clinical significance of NK cells for HIV-1 is supported by the fact that control of HIV-1 viremia is associated with HLA-C variants that interact with killer cell immunoglobulin-like receptor (KIR) proteins on the surface of NK cells (Lin et al., 2016b).

The experiments presented here examined the criteria that are used to define human ILCs. Consistent with the finding that all human ILCs, including NK cells, can be derived from a common Lin$^-$CD117$^+$ progenitor (Lim et al., 2017), significant deviation from the established markers for mouse ILCs was observed, setting the stage for detailed examination of the specific ILC subpopulations in human blood and colon lamina propria that are perturbed by HIV-1. Explanation for those abnormalities was sought, given that these cells lack requisite HIV-1 entry receptors and cannot be directly infected by HIV-1. What emerges is a greater understanding of the role that ILCs play in HIV-1-associated pathology and immunity, and of ILC plasticity more generally.

RESULTS

Major Populations of TBX21$^+$ and RORγT$^+$ ILCs are CD127$^-$

To identify ILCs from among human peripheral blood mononuclear cells (PBMCs), eleven cell surface proteins were used to exclude cells from other developmental lineages (Figures 1A, S1A, and S1B). Given that CD127 and EOMES are not reliable markers to distinguish human TBX21$^+$ILC1s from NK cells (Cortez et al., 2016; Gordon et al., 2012; Lim et al., 2017; Luther et al., 2003; Schmutz et al., 2009), and that the transcriptional profile of human CD94$^+$NK cells is distinct from that of CD94$^-$ILC1s and other ILCs (Björklund et al., 2016), and that several human ILC studies have used CD94 to exclude NK cells (Björklund et al., 2016; Hazenberg and Spits, 2014; Kløverpris et al., 2016), we used anti-CD94 to exclude NK cells from our ILC population (Figures 1A, S1A, and S1B). The remaining lineage negative (Lin$^-$) cells were then gated on TBX21 to define ILC1s, CRTH2 for ILC2s, and RORγT for ILC3s (Spits et al., 2013) (Figure 1B). No Lin$^-$TBX21$^+$RORγT$^+$ double-positive NKp44$^+$ILC3s (Hazenberg and Spits, 2014) were detected (Figures S1C and S2A), so ILC1 cells accounted for all Lin$^-$TBX21$^+$ cells.

Since CD127-positivity has been considered a defining characteristic of human ILCs (Björklund et al., 2016; Hazenberg and Spits, 2014; Ishizuka et al., 2016; Kløverpris et al., 2016) it was surprising that CD127$^-$TBX21$^+$ILC1s and CD127$^-$RORγT$^+$ILC3s were >100-fold more abundant than their CD127$^+$ counterparts (Figures 1B-1D and S2A-S2C). CRTH2$^+$ILC2s in the blood, though, were nearly all CD127$^+$ (Figure 1B). Analysis of eighteen proteins that had previously been reported in murine or human ILCs (Eberl et al., 2015; Hazenberg and Spits, 2014; Spits et al., 2013) demonstrated that CD127$^-$ ILCs are indeed a population that is distinct from CD127$^+$ILCs (Figure S2D). As was the case in adult peripheral blood, CD127$^-$TBX21$^+$ILC1s and CD127$^-$RORγT$^+$ILC3s were similarly abundant among umbilical cord blood mononuclear cells (Figures 1E, 1G, and 1H).

To determine if the high percentage of CD127$^-$ILCs was unique to blood, human colon lamina propria lymphoid cells were isolated from biopsies obtained at screening colonoscopy. The majority of human colon lamina propria ILC1s were CD127$^-$, as were a significant fraction of ILC3s (Figures 1F, 1I, and 1J). Many human blood and colon lamina propria ILCs, then, form distinct CD127$^-$ populations.

Among Blood ILCs, CD127$^-$ILC1s Are the Main Producers of Inflammatory Cytokines, and CD127$^-$ILC3s Do Not Make the Homeostatic Cytokine IL-22

ILCs influence biological processes via production of cytokines (Artis and Spits, 2015). Among human blood ILCs, CD127$^-$TBX21$^+$ILC1s were the main producers of IFN-γ, GM-CSF, or TNF-α (Figures 1K, 1L, S2E, and S2F). This was in contrast to the mouse where ILC3s are the main ILC subtype producing GM-CSF (Mortha et al., 2014). As expected, IL-13 was produced by CD127$^+$ILC2s (Figure 1M and S2F). IL-22 was not detected in blood ILC3s (Figure S2F), most of which were CD127$^-$ (Figures 1B, 1D). IL-22 was detected in lamina propria ILC3s (Figure 1M), most of which were CD127$^+$ (Figure 1F). These results indicate that IL-22 is only produced by those ILC3s that are CD127$^+$.

CD127$^+$ILCs and CD127$^-$ILC1s Are Reduced in the Blood and Colon Lamina Propria of HIV-1$^+$ People

To determine if CD127$^-$ or CD127$^+$ILCs are perturbed by HIV-1 infection, PBMCs from people with chronic HIV-1 infection were examined (Table S1). All CD127$^+$ILCs were decreased in the blood of people with HIV-1 infection (Figures 2A, 2B, 2D, 2G, and S3A), including CD127$^+$ILC3s (Figure 2E). CD127$^-$ILC1s were also reduced in the blood of HIV-1$^+$ individuals (Figures 2C, 2F, and S3B), though CD127$^-$ILC3s were not decreased (Figures 2E and 2H). The abnormalities in ILCs were significant ($p<0.01$) whether all HIV-1$^+$ samples were grouped together (Figures 2B, 2F, and 2G) or they were stratified based on either viremia or CD4 count (Figures S3C-S3H).

CD127$^+$ILCs were also decreased among lamina propria lymphoid cells isolated from the colon of HIV-1$^+$ individuals, despite anti-HIV-1 therapy with undetectable viremia

and normal numbers of lamina propria $CD4^+$T cells (Figures 2I, 2J, and S3I; Table S1). The majority of colon lamina propria ILC3s from HIV-1^- people were $CD127^+$ and these cells were decreased upon HIV-1 infection (Figures 2I and 2K). The effect of this abnormality would be expected to deprive the intestinal epithelium of homeostatic cytokines such as IL-22 (Figures 1M). This would disrupt the integrity of the colon epithelium and offer explanation for ongoing inflammation associated with HIV-1 infection (Deeks et al., 2013) (Figure 2L). Consistent with the observation in PBMCs, the frequency of colon $CD127^-$ILC3s did not decrease as a result of HIV-1 infection (Figure S3J).

Cytokines that Use the Common γ Chain Receptor Regulate the Plasticity of $CD127^+$ILCs via JAK3

To determine whether the decrease in $CD127^+$ILCs associated with HIV-1 infection might be a consequence of systemic elevation in cytokines or chemokines (Kacani et al., 1997; Roberts et al., 2010; Shebl et al., 2012; Stacey et al., 2009; Swaminathan et al., 2016), or of microbial contents leaking across the intestinal epithelium (Brenchley et al., 2006; Deeks et al., 2013), or of inflammatory markers such as the tryptophan-metabolite kynurinine (Favre et al., 2010), PBMCs and colon lamina propria lymphoid cells were stimulated *in vitro* and monitored by flow cytometry. The percentage of $CD127^+$ILCs was decreased by either PMA and ionomycin, the ILC1 stimulating cytokines IL-12 and IL-15 (Figures 3A, 3B and S4A), or IFN-β (Figure S4B). No significant change was observed after exposure to any of 16 additional cytokines, chemokines, TLR agonists, bacterial products, or kynurinine (Figures 3A, 3B, and S4B-S4F).

HIV-1 infection is associated with systemic elevation of cytokines that target the common γ chain receptor (Kacani et al., 1997; Roberts et al., 2010; Shebl et al., 2012; Stacey et al., 2009; Swaminathan et al., 2016). Given that IL-15 downregulated $CD127^+$ILCs (Figures 3A and 3B), the effect of other common γ chain cytokines was tested. IL-2, IL-4, IL-7, and IL-15, but not IL-9 or IL-21, down-regulated $CD127^+$ILCs (Figures 3C and S4G). That the $CD127^-$ILCs derive from $CD127^+$ILCs in our assay was

shown by tracking CD25, a protein found on CD127$^+$ILCs (Figures S2D and 3D). A JAK3 inhibitor, CP-690550, prevented CD127 downregulation by IL-7 or by IL-15 (Figure 3E), consistent with these cytokines signaling via the common γ chain (Leonard and O'Shea, 1998; Suzuki et al., 2000). JAK1/2 inhibitor ruxolitinib, and MTOR-inhibitor rapamycin, did not have this effect (Figures 3E and S4H). These results indicate that JAK3 signaling in response to systemic elevation of common γ chain cytokines likely decreases CD127$^+$ILCs in HIV-1 infection.

HIV-1 Reveals the Plasticity of CD127$^-$ILC1s

The experiments demonstrating reduction of CD127$^-$ILC1s by HIV-1 infection excluded NK cells by gating out CD94$^+$ cells (Figures 2C, 2F, S3B, S3D, S3G, S4I, and S4J). To distinguish CD127$^-$ILC1s from CD94$^+$NK cells, the anti-CD94 antibody was removed from our panel of lineage marker antibodies (hereafter denoted as *Lin). Under these conditions, the percentage of *Lin$^-$TBX21$^+$ cells, which included the sum of CD127$^-$ ILC1s and NK cells, was similar between HIV-1$^-$ and HIV-1$^+$ people (Figure S5A). As compared with CD127$^-$ILC1s, though, the percentage of CD94$^+$ NK cells in the *Lin$^-$ TBX21$^+$ population was increased in the blood of HIV-1$^+$ individuals (Figures 4A and 4B). This abnormality was evident whether blood was examined from individuals with CD4 cells >500/mm^3 or <500/mm^3 or with viremia >10^4/ml or <10^2/ml (Figures S5B and S5C).

Stimulation of PBMCs with PMA and ionomycin, IL-15, or IL-12 + IL-15, caused an increase in the ratio of CD94$^+$NK cells to CD127$^-$ILC1s, similar that observed with HIV-1 infection (Figures 4C, 4D, S5D and S5E). In our assay, the levels of Ki67 and Annexin V were similar on the CD127$^-$ILC1s and CD94$^+$NK cells, suggesting that observed differences in percentages of these cells *in vivo* do not result from intrinsic differences in the rates of proliferation or apoptosis (Figures S5F-S5H).

Though ILC1s and NK cells are considered developmentally distinct in the mouse (Klose et al., 2014; Spits et al., 2016), all human ILCs, including NK cells, can be derived from a common Lin$^-$CD117$^+$ progenitor (Lim et al., 2017). In keeping with this

observation, our results above suggested that human CD127$^-$ILC1s become NK cells in response to immune stimulation. ILC plasticity has been demonstrated for CRTH2$^+$ILC2s and RORγT$^+$ILC3s, either of which may become CD127$^+$TBX21$^+$ILC1s (Bernink et al., 2015; Lim et al., 2016). To test whether CD127$^-$ILC1s also exhibit such plasticity, CD127$^-$ILC1s were sorted by flow cytometry (Figure S5I) and stimulated *in vitro* with PMA and ionomycin, or with IL-12 and IL-15. In response to stimulation, CD127$^-$ILC1s became CD94$^+$NK cells (Figures 4E-4G and S5J) with increased degranulation activity (Figures 4H and S5K). In the absence of exogenous stimulation, CD94$^+$NK cells sorted directly from blood had greater killing activity than did CD127$^-$ ILC1s (Figure 4I). Thus, like other ILC subsets (Bernink et al., 2015; Lim et al., 2016), CD127$^-$ILC1s exhibit plasticity, with the ability to become functional CD94$^+$NK cells in response to stimulation.

To better understand the molecular basis for CD127$^-$ILC1s becoming CD94$^+$NK cells, RNA-Seq was performed with CD127$^-$ILC1s and NK cells sorted from two donors. As compared with CD94$^+$NK cells, CD127$^-$ILC1s expressed 70 genes at higher level and 140 genes at lower level (Figure 4J; Table S2). Consistent with the observation that CD94$^+$NK cells result from stimulation of CD127$^-$ILC1s, CD44, CD2, and CXCR3, as well as cytolytic molecule GZMK, were expressed at higher level on CD94$^+$NK cells (Figure 4J). Proteins encoded by nine of the differentially expressed genes were confirmed to be produced in a correspondingly differential manner by flow cytometry (Figure 4K).

CD127$^-$ILC1s are Precursors of TCF7$^+$NK Cells

Single-cell RNA-Seq by high-content, droplet barcoding (Klein et al., 2015) was used to capture the transcriptome of individual cells across the spectrum from CD127$^-$ILC1s to CD94$^+$NK cells (Figures 5A, S6A; Table S3). CD94 was used to identify NK cells (Hazenberg and Spits, 2014) but transcriptional profiling indicated that this cell surface protein was not sufficient to separate all CD94$^+$NK cells from CD127$^-$ILC1s (Figure 5A). Interestingly, CD94 mRNA levels were identical in CD127$^-$ILCs and NK cells, indicating that CD94 protein synthesis is primarily regulated post-transcriptionally (Figure S6B).

In contrast, unbiased clustering, ignoring whether or not a given cell was CD94$^+$, showed two distinct cell populations (Figure 5B). The validity of clustering cells into two groups was confirmed by calculating prediction strength as a function of cluster number (Tibshirani and Walther, 2005) (Figure S6C). Cluster 1 was homogeneous and consisted of 396 CD94$^+$NK cells (Figure 5B, lower left). Cluster 2 contained 371 CD94$^+$NK cells and 973 CD127$^-$ILC1s (Figure 5B, upper right). A heatmap was created based on the transcriptome of 3,277 single cells collected from two donors, utilizing all differentially expressed genes from the spectral cluster analysis (Figure 5C; Table S4). This showed a clear shift in the pattern of gene expression along the continuum of CD94 expression (see blue and yellow bars at the top of Figure 5C) .

To determine whether the observed heterogeneity in the individual CD127$^-$ILC1 transcriptomes was a reflection of cells caught at different stages in the CD127$^-$ILC1 to NK cell transition, a minimum spanning tree was constructed using Monocle (Trapnell et al., 2014) based upon the transcriptome of individual cells (Figure 5D). When the heatmap was reconstructed utilizing the pseudotime ordering of single cells based on the minimum spanning tree (Figure S6D), the pattern was nearly indistinguishable from the heatmap ordered by hierarchical clustering (Figure 5C), confirming the validity of arranging cells along the transcriptional timeline that had been assigned by the minimum spanning tree.

Differential expression analysis based on the pseudotemporal ordering of cells from the minimum spanning tree was used to identify genes that regulate the transition from CD127$^-$ILC1s to CD94$^+$ NK cells. TCF7, a gene that encodes a WNT pathway transcription factor (Nusse and Clevers, 2017) critical for memory CD8$^+$ memory T cells (Utzschneider et al., 2016), was only expressed in the homogeneous NK cell cluster (Figure 5E, 5F; $p < 7 \times 10^{-103}$). Similar differential expression patterns were observed for CD44, a gene important for T cell survival and establishment of memory cells (Baaten et al., 2010) (Figure 5F), for PIM3, a serine-threonine kinase that blocks apoptosis and

promotes self-renewal (Aksoy et al., 2007), and for CD62L, GZMK, and CXCR3 (Figures 5F).

TCF7^{+}NK cells examined by flow cytometry were exclusively CD56^{hi} (Figure S6E), a marker for NK cells with capacity to proliferate and differentiate into CD56^{dim} effector NK cells (Moretta, 2010). CXCR6, a gene required for memory NK cell generation in response to haptens and viruses (Paust et al., 2010) was also highly enriched on TCF7^{+}NK cells, as were CD44, CD62L and CXCR3 (Figure S6E).

The effect of cytokine stimulation on the NK cell markers identified by RNA-Seq was examined next. When sorted CD127^{-}ILC1s were stimulated with IL-12 and IL-15 to become CD94^{+}, the cells also became TCF7^{+} (Figures S7A and 5G) and upregulated CD44, CXCR3, CXCR6, and GZMK (Figure 5G). When sorted TCF7^{+}NK cells were stimulated with cytokines, TCF7 was downregulated on those cells that proliferated (Figure S7A and S7B), analogous to CD8^{+} memory T cells that downregulate TCF7 when stimulated to divide (Lin et al., 2016a). TCF7, then, defines an NK subset that bears cell surface markers of memory NK cells and T cells.

WNT Inhibition Blocks the Cytokine Induced Transition of CD127^{-}ILC1 into NK Memory Cells

To determine if TCF7 drives the cytokine-stimulated transition of CD127^{-}ILC1s into NK cells, PBMCs or sorted CD127^{-}ILC1s were treated with LGK974, a potent but non-toxic inhibitor of WNT signaling (Liu et al., 2013) that is currently being tested in clinical trials (https://clinicaltrials.gov/ct2/show/NCT01351103). LGK974 blocked the cytokine-induced transition of CD127^{-}ILC1s to NK cells, as evidenced by blockade of induction of the NK cell specific markers CD94, CD44, CXCR3 and CD56^{hi} (Poli et al., 2009) (Figures 6A-6F and S7C-S7E). The effect of LGK974 was specific in that the drug caused no signs of toxicity when cells were examined following culture in the drug for 16 hrs or eight days, with or without stimulation (Figure S7F); in the absence of stimulation, LGK974 alone caused no change in the CD94^{-}/CD94^{+} ratio within the *Lin^{-}TBX21^{+} population (Figure S7F); in the presence of stimulation, total CD56 was not changed by

LGK974 (Figure S7F); and M-110, an inhibitor of the NK cell kinase PIM3 (Figures 5C and 5F), had no effect on the cytokine-induced transition from CD127$^-$ILC1s to NK cells (Figure S7G). These experiments provide evidence that TCF7 is required for the cytokine-induced transition of CD127$^-$ILC1s to NK cells.

The capacity of CD127$^-$ILC1s to generate functional NK memory cells, and the role of TCF7 in this process, was assessed using an established protocol (Cooper et al., 2009; Romee et al., 2012), that is shown schematically in Figure S7H. ILCs received a primary stimulus of IL-12, IL-15, and IL-18 for 16 hrs and then cells were rested in IL-15 alone. After five days, cells were re-stimulated with IL-12 and IL-15 and heightened IFN-γ production was considered a readout for an anamnestic response (Figure S7I). LGK974 strongly inhibited the IFN-γ memory response in all 13 donors tested (Figure 6G and 6H) demonstrating that TCF7 is required for the cytokine-induced NK cell memory response, attributable to CD127$^-$ILC1 plasticity.

Expansion of TCF7$^+$ Memory NK Cells in HIV-1 Infection

In blood from HIV-1 negative people, TCF7 was detected in CD94$^+$NK cells but not in CD127$^-$ILC1s (Figures 4K, 5E, 5F, S6E, 7A and 7B). In contrast, in blood from HIV-1$^+$ people, the TCF7$^+$CD94$^+$NK cell population was greatly increased and TCF7 was even detectable among CD127$^-$ILC1s (Figures 7A and 7B), indicating that HIV-1-induced immune activation increased the memory NK cell population. This newly described plasticity of CD127$^-$ILC1s, driven by TCF7, offers explanation for the increased NK cell memory reported with HIV-1 infection (Cerwenka and Lanier, 2016; Reeves et al., 2015). Additionally, NKG2C, a C-type lectin protein that is upregulated on memory NK cells specific for human cytomegalovirus (Lee et al., 2015) was also elevated by HIV-1 infection (Figure 7C and 7D). Thus, CD127$^-$ILC1 plasticity driven by TCF7 may serve as a common mechanism for memory NK cell formation in different contexts. Analogous to the effector memory T cells that are increased with HIV-1 infection (Massanella et al., 2015), TCF7$^+$ memory NK cells and effector NK cells both likely derive from the response of CD127$^-$ILC1s to immune stimulation (Figure 7E).

DISCUSSION

Studies on human tissues have largely used cell surface CD127 as necessary criterion for defining cells as ILCs (Björklund et al., 2016; Hazenberg and Spits, 2014; Kløverpris et al., 2016; Spits et al., 2013). The experiments reported here show that this practice has consequences for understanding ILC biology in the context of human pathology. The vast majority of ILC1s and ILC3s in the blood, as well as most ILC1s and many ILC3s in the colon lamina propria, are, surprisingly, CD127$^-$ (Figures 1B-1D, 1F, 1I and 1J). Additionally, these cells constituted the majority of cord blood ILCs (Figures 1E, 1G and 1H). CD127$^-$ILCs differed from their CD127$^+$ counterparts with respect to a number of cell surface markers (Figure S2D). Given the relatively high percentage of CD127$^-$ ILCs, these cells clearly should not be excluded from analysis. More importantly, the assessment of these populations within the context of HIV-1 infection that is reported here offered insight into the mechanisms underlying inflammatory pathology and revealed plasticity of ILC subsets that was not otherwise evident.

The non-AIDS, inflammatory pathology associated with HIV-1 infection is attributed, at least in part, to chronic disruption of the intestinal epithelium (Brenchley et al., 2006). The integrity of the epithelium is maintained by homeostatic cytokines such as IL-22 that are produced by ILC3s (Cella et al., 2009; Zheng et al., 2008). The experiments here demonstrate ILC abnormalities within the colon lamina propria of people who are on effective antiviral treatment for chronic HIV-1 infection. Given that blood CD127$^+$ILCs are disrupted soon after HIV-1 infection (Kløverpris et al., 2016) it is likely that the abnormalities in the colon lamina propria CD127$^+$ILCs detected here are also established early, during acute HIV-1 infection. The specific abnormalities that were detected here provide insight into the etiology and mechanism underlying this persistent pathology. CD127$^+$ILC3s, but not CD127$^-$ILC3s, were depleted from the colon (Figures 2K and S3J). IL-22 production was readily detected among CD127$^+$ILC3s, but not in CD127$^-$ILC3s. These observations, diagramed schematically in Figure 2L, offer explanation for ongoing inflammation with chronic HIV-1 infection.

CD127$^+$ILCs appear not to be eliminated as a result of direct infection by HIV-1. These cells lack HIV-1 entry receptors and challenge with HIV-1 yielded negative results for

productive infection, in our hands and those of others (Kløverpris et al., 2016). The cause for the specific disruption of CD127^{+}ILCs in response to HIV-1 infection was sought here from among 26 factors - cytokines, chemokines, and bacterial products - that have been reported to be elevated systemically with HIV-1 infection (Brenchley et al., 2006; Deeks et al., 2013; Favre et al., 2010; Kacani et al., 1997; Roberts et al., 2010; Shebl et al., 2012; Stacey et al., 2009; Swaminathan et al., 2016). It was found that IL-2, IL-4, IL-7, and IL-15, all cytokines that signal through the common gamma chain receptor in a JAK3-dependent fashion (Leonard and O'Shea, 1998; Suzuki et al., 2000) downregulated CD127 on ILCs (Figures 3C and 3E). These findings, along with the persistence of CD127^{-}ILC3s in the blood and colon of HIV-1^{+} people whose CD127^{+}ILCs were decreased, indicate that, rather than simply being eliminated by HIV-1 infection, ILCs downregulate CD127, and the phenotype of these cells changes in response to inflammatory cytokines. Though IL-7 and its cognate receptor, CD127, are considered essential for ILC development (Spits and Di Santo, 2011; Vonarbourg and Diefenbach, 2012), CD127 is apparently not required for maintenance of all ILC subtypes. The number of lymphoid-tissue-inducer (LTi) cells, a subset of ILC3s, was normal in blood and spleen of newborn CD127$^{-/-}$ or IL-7$^{-/-}$ mice (Luther et al., 2003; Schmutz et al., 2009). Better understanding of the plasticity of the lamina propria ILC populations, and loss of their homeostatic function in response to inflammation, may lead to new therapies that limit the inflammatory sequelae of HIV-1 infection and other diseases.

HIV-1 infection was associated with reduction in the percentage of blood CD127^{-}ILC1s (Figures 2C and 2F) and this was accompanied by an increase in the percentage of CD94^{+}NK cells (Figures 4A and 4B). *In vitro* stimulation of CD127^{-}ILC1s from HIV-1^{-} blood converted these cells into CD94^{+}NK cells with increased degranulation activity and cytotoxicity (Figures 4E-4I), in agreement with the increased cytotoxic activity others have reported for CD94^{+}NK cells (Davis et al., 2016; Yu et al., 2009), and the finding that all human ILCs, including NK cells, can be derived from a common Lin^{-} CD117^{+} progenitor (Lim et al., 2017), The CD94^{+}NK cells, which included CD56^{hi}NK cells, bore higher levels of activation markers than did CD127^{-}ILC1s (Figures 4J and

4K). The data indicate that, rather than being killed off by HIV-1 infection, CD127$^-$ILC1s are converted into CD94$^+$NK cells by HIV-1 associated inflammation.

Clustering of transcriptomes from thousands of individual cells from HIV-1$^-$ blood revealed a pseudotime developmental trajectory (Trapnell et al., 2014) from CD127$^-$ ILC1s to CD94$^+$NK cells that tracked with expression of the WNT transcription factor TCF7 (Figure 5D). Reverse genetic experiments attempting to perturb the function of TCF7 were attempted but the titer of lentiviral or AAV vectors on human CD127$^-$ILC1s was too low to generate statistically significant phenotypes. Instead, LGK974, a WNT inhibitor of clinical utility was exploited to show that this signaling pathway drives the CD127$^-$ILC1 to NK cell transition and the establishment of NK cell memory (Figures 5 and 6).

The TCF7$^+$NK cells that were enriched with HIV-1 infection had markers that have been reported for memory NK cells, including CD44, CXCR6, NKG2C and CD94. (Figure 7C, 7D and S6E). One of the hallmarks of memory lymphoid cells is the ability to proliferate quickly with enhanced effector function upon restimulation. The TCF7$^+$ cells were CD56^{hi} (Figure S6E), a population of NK cells that exhibits the highest proliferation ability among NK subsets (Caligiuri 2008). TCF7 regulates CD44 expression (van de Wetering et al., 2002) and the developmental trajectory in Figures 5D and 5E indicates that TCF7 is critical for establishment of these memory-associated NK markers. The increase in CD94$^+$NK cells (Figures 4A and 4B) and in TCF7$^+$NK cells (Figures 7A and 7B) that was observed with HIV-1 infection may very well account for the reported increase in NK cell memory responses with this infection (Deeks, 2011; Paust et al., 2010). TCF7/WNT signaling inhibitor LGK974, which inhibited immune stimulation induced transition of CD127$^-$ILC1 to NK cells and the establishment of memory NK cells with increased IFN-γ response to secondary stimulation, might offer clinical benefit in treating HIV-1 related chronic inflammation. Taken together, these experiments indicate that the shift from CD127$^-$ILC1s to CD94$^+$NK cells that was observed with HIV-1 infection reflects ILC plasticity that is part of normal NK cell physiology.

MATERIALS AND METHODS

Clinical samples. All human blood and colon samples were collected from participants who had provided written informed consent for protocols that included study of cellular immunity in HIV-1 infection, in accordance with procedures approved by the University of Massachusetts Medical School (UMMS) Institutional Review Board. Routine screening colonoscopy was scheduled as medically indicated. HIV-1$^-$ control individuals undergoing colonoscopy the same day were matched for gender and age. In pilot experiments with two patients, multiple biopsies of different segments of the bowel from the same patient were compared and no differences in ILC populations were found. Subsequent sampling was from the descending colon only. All patients were consented the day of the procedure. All blood and colon samples that were collected and processed were included in the data analysis after simple allocation into one of two groups, HIV-1$^-$ or HIV-1$^+$. Attempts to stratify samples according to viral load or CD4$^+$ T cell count of the donor failed to detect significant differences between the subgroups (Figures S3 and S5).

Antibodies and reagents. The antibodies and reagents used in this study was included in Table S5 and Table S6.

Human mononuclear cell isolation. Human peripheral blood or umbilical cord blood was diluted with an equal volume of RPMI-1640 (Gibco), overlaid on Histopaque (Sigma), and centrifuged at 500 x g for 30 mins at room temperature. Mononuclear cells were washed 3 times with MACS buffer (0.5% BSA and 2 mM EDTA in PBS) and either used immediately or frozen in FBS containing 10% DMSO.

Human intestinal lamina propria lymphoid cell (LPL) preparation. Human intestinal biopsies were incubated with PBS containing 5 mM EDTA, 150 μg/ml DTT, and 0.1% β-mercaptoethanol on a shaker for 15 min at 37℃ to remove epithelial cells. The remaining tissue containing the LPLs was washed with complete RPMI-1640 (10% FBS, 1:100 GlutaMAX, and 1:1000 β-mercaptoethanol), then digested with RPMI-1640

containing 125 μg/ml Liberase (Roche) and 200 μg/ml DNase I (Sigma) for 30 min on a shaker at 37℃. LPLs were filtered through a 70 μm cell strainer and washed with RPMI-1640.

Definition of human lineage-negative lymphoid populations. Live singlets of human PBMCs, or of intestinal lamina propria lymphoid cells, were stained with a panel of lineage markers (Lin): anti-CD3, anti-TCRαβ, anti-CD19, anti-B220, anti-CD34, anti-FcεRIα, anti-CD11c, anti-CD303, anti-CD123, anti-CD1a, anti-CD14, and anti-CD94. The specific antibodies used are listed in Table S5. Cells that were negative for all lineage markers were defined as lineage-negative (Lin^-) lymphoid cells. As indicated in some experiments, the anti-CD94 antibody was not included in the antibody panel; cells that were negative after staining with these antibodies were designated $*Lin^-$.

Human $CD127^-$ILC1 and NK cell enrichment. $CD127^-$ILC1s and NK cells were negatively enriched by excluding T cells, B cells, stem cells, dendritic cells, monocytes, granulocytes, and erythroid cells with the human NK isolation kit (MACS) according to manufacturer's instruction.

Flow cytometry. Live and dead cells were discriminated using the Live and Dead violet viability kit (Invitrogen, L-34963). For cell surface molecule detection, the cells were resuspended in antibody-containing MACS buffer for 30-60 min at 4°C in the dark. To detect cytokine production, cells were stimulated with the indicated cytokines for 16 hrs, or with PMA and ionomycin (cell stimulation cocktail 00-4970-03, ebioscience) for 3-6 hrs. In both cases, protein transport inhibitor (00-4980-03, eBioscience) was present during the stimulation. For intracellular staining of transcription factors or cytokines, cells were fixed and permeabilized using Foxp3 staining buffer kit (eBioscience) and target intracellular molecules were stained as for surface staining.

Cell sorting. PBMCs were stained with a panel of lineage markers that included anti-CD3, anti-TCRαβ, anti-CD19, anti-B220, anti-CD34, anti-FcεRIα, anti-CD11c, anti-CD303, anti-CD123, anti-CD1a, and anti-CD14. The lineage negative population was

designated *Lin$^-$ to distinguish it from the full Lin$^-$ population which additionally included the anti-CD94 antibody. For sorting, *Lin$^-$ cells were then stained with anti-CD56 and anti-CD94 antibodies. CD127$^-$ILC1s (*Lin$^-$CD56$^+$CD94$^-$), total NK cells (*Lin$^-$CD56$^+$CD94$^+$) and TCF7$^+$NK cells (*Lin$^-$CD56^{hi}CD94$^+$) were sorted using a BD FACSAria IIu.

Degranulation assay. PBMCs were seeded in a 24 well plate at 2 × 10^6 cells/well in RPMI-1640 with anti-CD107a antibody (Biolegend, 1:200). Then, cells were treated with PMA/ionomycin and protein transport inhibitor for 5 hrs in a 37℃ incubator with 5% CO_2. Surface CD107a was detected by flow cytometry.

Killing assay. K562 or Jurkat cells were washed and resuspended at 10^6 cell/ml in PBS. Calcein-AM (Neri et al., 2001) (Molecular Probes) was added at 10 μM and the cells were labelled at 37°C in 5% CO_2 for 30 min. After washing with PBS for 2 times, the labelled cells were resuspended in complete RPMI-1640 and aliquoted in a V bottom 96 well plate (5,000 cells in 100 μl). The sorted ILC1 or NK cells were resuspended in complete RPMI-1640 and the concentration was adjusted at 15 fold of target cells (7.5×10^4 cells) in 50μl. The effector and target cells were mixed and centrifuged at 50 x g for 0.5 min and were incubated at 37°C in 5% CO_2 for 6 hrs. Cells were pelleted and 100 μl supernatant was transferred to a 96-well solid black microplate. The fluorescence released by labelled target cells were detected using BioTek Synergy 2 plate reader (excitation filter: 485/20 nm; band-pass filter: 528/20 nm). Specific lysis was determined as: [(test fluorescence release - spontaneous fluorescence release) / (maximum fluorescence release - spontaneous fluorescence release)] × 100.

Real-time quantitative PCR (qRT-PCR). The RNA of sorted CD127-ILC1s and NK cells were extracted using TRIzol reagent (invitrogen, 15596018) according to manufacturer's instruction. Reverse transcription were performed using SuperScript VILO Master Mix (invitrogen, 11755050), and CD94 mRNA level were determined by

qRT-PCR, using taqman probe (Applied Biosystems, Hs00233844_m1), GAPDH were detected as an internal control (Applied Biosystems, Hs03929097_g1).

Library preparation for bulk RNA-Seq. The bulk RNA sequencing library was prepared using CEL-Seq2 (Hashimshony et al., 2016). RNA of sorted cells was extracted using TRIzol reagent. 10 ng RNA was used for first strand cDNA synthesis using barcoded primers containing unique molecular identifier (UMI) sequences. Specifically, the RNA of CD127^{-}ILC1s was reverse transcribed with 5'-GCC GGT AAT ACG ACT CAC TAT AGG GAG TTC TAC AGT CCG ACG ATC NNN NNN AGA CTC TTT TTT TTT TTT TTT TTT TTT TTT V-3' and 5'-GCC GGT AAT ACG ACT CAC TAT AGG GAG TTC TAC AGT CCG ACG ATC NNN NNN CAG ATC TTT TTT TTT TTT TTT TTT TTT TTT V-3'. The RNA of CD94^{+}NK cells was reverse transcribed with 5'-GCC GGT AAT ACG ACT CAC TAT AGG GAG TTC TAC AGT CCG ACG ATC NNN NNN CAT GAG TTT TTT TTT TTT TTT TTT TTT TTT V-3' and 5'-GCC GGT AAT ACG ACT CAC TAT AGG GAG TTC TAC AGT CCG ACG ATC NNN NNN TCA CAG TTT TTT TTT TTT TTT TTT TTT TTT V-3'. The second strand was synthesized using NEBNext Second Strand Synthesis Module (NEB). The pooled dsDNA was purified with AMPure XP beads (Beckman Coulter, A63880) and subjected to in vitro transcription (IVT) using HiScribe T7 High Yield RNA Synthesis Kit (NEB), then treated with ExoSAP-IT (Affymetrix 78200). IVT RNA was fragmented using RNA fragmentation reagents (Ambion) and underwent a 2nd reverse transcription step using randomhexRT primer-5'-GCC TTG GCA CCC GAG AAT TCC ANN NNN N-3' to incorporate the second adapter. The final library was amplified with indexed primers: RP1-5'-AAT GAT ACG GCG ACC ACC GAG ATC TAC ACG TTC AGA GTT CTA CAG TCC GA-3' and RPI1-5'-CAA GCA GAA GAC GGC ATA CGA GAT CGT GAT GTG ACT GGA GTT CCT TGG CAC CCG AGA ATT CCA-3' and the purified library was quantified with 4200 TapeStation (Agilent Technologies) and paired-end sequenced on a Nextseq 500 V2 (Illumina) using 15 cycles Read 1, 6 cycles Index 1, and 71 cycles Read 2.

Library preparation for single cell RNA-Seq. The single cell sequencing library was prepared using InDrop barcoding (Klein et al., 2015). Individual, pre-sorted cells were

captured in droplets containing lysis buffer, reverse transcription reagents, and hydrogel microspheres carrying primers for barcoding, each captured cell using a custom-built InDrop microfluidics system, as described (Klein et al., 2015). After cDNA for each cell was synthesized in individual droplets with unique barcodes, the droplet emulsion was broken and cDNA from all cells was pooled. A single cell cDNA library was prepared using essentially CEL-Seq2 (Hashimshony et al., 2016) as described above for bulk RNA-Seq, with the following changes. PE2-N6-5'-TCG GCA TTC CTG CTG AAC CGC TCT TCC GAT CTN NNN NN-3' was used in the 2nd reverse transcription reaction. CD127^{-}ILC1 libraries were linearly amplified with Indexed primers PE1-6: 5'-CAA GCA GAA GAC GGC ATA CGA GAT ATT GGC CTC TTT CCC TAC ACG A-3' or PE1-17: 5'-CAA GCA GAA GAC GGC ATA CGA GAT CTC TAC CTC TTT CCC TAC ACG A-3' and PE2: 5'-AAT GAT ACG GCG ACC ACC GAG ATC TAC ACG GTC TCG GCA TTC CTG CTG AAC-3'. Libraries from CD94^{+}NK cells were amplified with index 1 primers PE1-12: 5'-CAA GCA GAA GAC GGC ATA CGA GAT TAC AAG CTC TTT CCC TAC ACG A-3' or PE1-18: 5'-CAA GCA GAA GAC GGC ATA CGA GAT GCG GAC CTC TTT CCC TAC ACG A-3', and PE2 (above). Libraries were sequenced 38 cycles Read 1, 6 cycles Index 1, 48 cycles Read 2 using Illumina Nextseq 500 V2 with custom sequencing primers added to the cartridge: R1 5'-GGC ATT CCT GCT GAA CCG CTC TTC CGA TCT-3' Idx: 5'-AGA TCG GAA GAG CGT CGT GTA GGG AAA GAG-3' R2 5'-CTC TTT CCC TAC ACG ACG CTC TTC CGA TCT-3'.

Bulk RNA-Seq Processing and Analysis. The four pooled sets of RNA-Seq reads were separated by CEL-Seq barcodes and mapped to the HG19 genome using Tophat (Kim et al., 2013) (version 2.0.14, default parameters). Aligned reads were quantified by ESAT (Derr et al., 2016) using a transcript annotation file containing all RefSeq genes filtered to select only 'NM' transcripts and extending the transcripts up to 1,000 bases past the end of the annotated 3' end (*-wExt 1000, -task score3p*), discarding multimapped reads (*-multimap ignore*). Differential expression analysis was performed using DESeq2 (Love et al., 2014), contrasting the CD127^{-}ILC1 samples with the CD94^{+}NK cell samples. Differentially expressed genes were selected if the log2 fold-change was greater than 1.0, with $p < 0.05$.

Single cell RNA-Seq processing and analysis. Reads were mapped to the HG19 genome using Tophat (Kim et al., 2013) (version 2.0.14, default parameters). To assign each read to a given cell and collapse duplicate reads into single UMIs, alignments were processed by ESAT (Derr et al., 2016) using its single-cell analysis module (*-scPrep*) with the same transcript annotation file used for the bulk RNA-Seq analysis, extending the transcripts up to 1,000 bases past the annotated 3' end (*-wExt 1000, -task score3p*), discarding multimapped reads (*-multimap ignore*), and requiring a single observation of a UMI for a transcript to be counted (*-umiMin 1*).

The final output of ESAT is a table where rows are genes, cells are columns, and values represent the number of UMIs detected in each cell. The dataset was loaded into R and the packages used (if not part of base R) are noted. First, data was normalized using the TMM method from EdgeR (Robinson and Oshlack, 2010). On this matrix, PCA was run in order to determine the number of dimensions that contribute variance to the data and to select genes that were highly variable in the dataset. ICA was run using the fastICA (Hyvärinen and Oja, 2000) algorithm to reduce the data to the number of dimensions that contained variance. To determine the optimum number of cell clusters in the dataset the methods of (Tibshirani and Walther, 2005) were utilized. This analysis showed 2 clusters gives the highest predictive strength, and that further subdividing of the cells into additional clusters severely lowered the score. Spectral clustering was then run with n of 2 centers and the symmetrical method on the cell's ICA components using the kknn package (Hechenbichler and Schliep, 2004). For visualization, the cells were then reduced to 2 dimensions using the Rtsne package, which took the ICA components as input (Van Der Maaten, 2014). Lastly, the minimum spanning tree (MST) was constructed on the tSNE plot utilizing Monocle (Trapnell et al., 2014). For pseudotime analysis, Monocle's built-in differential expression tools were utilized. For visualization purposes, tSNE mapped cells were color coded by the expression of given genes; a weighted density map was created that takes into account both the number of cells in a region as well as their expression values.

Cytokine induced ILC1 and NK cell memory assay. PBMCs or enriched CD127$^-$ILC1 and NK cells were pre-stimulated with IL-15 (5 ng/ml) + IL-12 (10 ng/ml) + IL-18 (50 ng/ml) for 16 hrs, or cells were incubated with IL-15 alone (5 ng/ml) to maintain cell survival (no pre-stimulation, control). Cytokines were washed out and the cells were rested by incubation in IL-15 (5 ng/ml) alone for 5 days. Cells were then re-stimulated with IL-12 (50 ng/ml) + IL-15 (50 ng/ml) for 16 hrs. IFN-γ production was detected by intracellular staining with anti-IFN-γ antibody using a Foxp3 staining buffer kit (eBioscience). As compared with cells that had not been pre-stimulated, the increase in IFN-γ production in pre-stimulated cells was used as a readout for pre-stimulation induced memory, as previously described (Poli et al., 2009).

Statistics. Statistical analysis was performed with GraphPad Prism software using paired or unpaired two-tailed student's *t*-test as indicated in the figure legends. $p<0.05$ was considered as significant. Variance was estimated by calculating the mean ± s.e.m. in each group. Variances among groups of samples were compared using the F-test function in GraphPad.

RNA-Seq datasets. Our RNA-Seq datasets, including bulk and single cell RNA-Seq for the two FACS sorted cell populations, from two blood donors, has GEO accession number GSE97727, and can be found at:
https://www.ncbi.nlm.nih.gov/geo/query/acc.cgi?acc=GSE97727

ACKNOWLEDGEMENTS

We thank the patients who generously provided blood and colon biopsy samples, as well as their caretakers, Drs. Jennifer Daly, Sarah Cheeseman, and Mireya Wessolossky of the University of Massachusetts Medical School (UMMS). Caitlin Mannarino, Anne Foley, and Margaret McManus (UMMS) provided IRB regulatory assistance, sample preparation, and record keeping. Katherine Luzuriaga (UMMS) supported the patient sample database and repository. Alex Ratner, Sarah Boswell, and Allon Klein (Harvard Medical School) contributed technical assistance and barcoded hydrogel beads. David Artis, Leslie Berg, Marco Colonna, Jun Huh, Joonsoo Kang, and Susan Swain offered invaluable advice. This research was supported by NIH U01HG007910 (to M.G. and J.L.), R01AI111809 (to J.L.), DP1DA034990 (to J.L.), R21AI119885 (to M.G.), R01DK105837 (to M.G.), and the Translational Medicine Core of the University of Massachusetts Center for AIDS Research (P30AI042845).

REFERENCES

Aksoy, I., Sakabedoyan, C., Bourillot, P.-Y., Malashicheva, A.B., Mancip, J., Knoblauch, K., Afanassieff, M., and Savatier, P. (2007). Self-Renewal of Murine Embryonic Stem Cells Is Supported by the Serine/Threonine Kinases Pim-1 and Pim-3. Stem Cells *25*, 2996–3004.

Alter, G., Heckerman, D., Schneidewind, A., Fadda, L., Kadie, C.M., Carlson, J.M., Oniangue-Ndza, C., Martin, M., Li, B., Khakoo, S.I., et al. (2011). HIV-1 adaptation to NK-cell-mediated immune pressure. Nature *476*, 96–100.

Artis, D., and Spits, H. (2015). The biology of innate lymphoid cells. Nature *517*, 293–301.

Baaten, B.J.G., Li, C.-R., Deiro, M.F., Lin, M.M., Linton, P.J., and Bradley, L.M. (2010). CD44 regulates survival and memory development in Th1 cells. Immunity *32*, 104–115.

Bernink, J.H., Krabbendam, L., Germar, K., de Jong, E., Gronke, K., Kofoed-Nielsen, M., Munneke, J.M., Hazenberg, M.D., Villaudy, J., Buskens, C.J., et al. (2015). Interleukin-12 and -23 Control Plasticity of CD127+ Group 1 and Group 3 Innate Lymphoid Cells in the Intestinal Lamina Propria. Immunity *43*, 146–160.

Björklund, Å.K., Forkel, M., Picelli, S., Konya, V., Theorell, J., Friberg, D., Sandberg, R., and Mjösberg, J. (2016). The heterogeneity of human CD127(+) innate lymphoid cells revealed by single-cell RNA sequencing. Nat. Immunol. *17*, 451–460.

Brenchley, J.M., Price, D.A., Schacker, T.W., Asher, T.E., Silvestri, G., Rao, S., Kazzaz, Z., Bornstein, E., Lambotte, O., Altmann, D., et al. (2006). Microbial translocation is a cause of systemic immune activation in chronic HIV infection. Nat. Med. *12*, 1365–1371.

Cella, M., Fuchs, A., Vermi, W., Facchetti, F., Otero, K., Lennerz, J.K.M., Doherty, J.M., Mills, J.C., and Colonna, M. (2009). A human natural killer cell subset provides an innate source of IL-22 for mucosal immunity. Nature *457*, 722–725.

Cerwenka, A., and Lanier, L.L. (2016). Natural killer cell memory in infection, inflammation and cancer. Nat. Rev. Immunol. *16*, 112–123.

Cooper, M.A., Elliott, J.M., Keyel, P.A., Yang, L., Carrero, J.A., and Yokoyama, W.M. (2009). Cytokine-induced memory-like natural killer cells. Proc. Natl. Acad. Sci. U. S. A. *106*, 1915–1919.

Cortez, V.S., Cervantes-Barragan, L., Robinette, M.L., Bando, J.K., Wang, Y., Geiger, T.L., Gilfillan, S., Fuchs, A., Vivier, E., Sun, J.C., et al. (2016). Transforming Growth Factor-β Signaling Guides the Differentiation of Innate Lymphoid Cells in Salivary Glands. Immunity *44*, 1127–1139.

Davis, Z.B., Cogswell, A., Scott, H., Mertsching, A., Boucau, J., Wambua, D., Le Gall,

S., Planelles, V., Campbell, K.S., and Barker, E. (2016). A Conserved HIV-1-Derived Peptide Presented by HLA-E Renders Infected T-cells Highly Susceptible to Attack by NKG2A/CD94-Bearing Natural Killer Cells. PLoS Pathog. *12*, e1005421.

Deeks, S.G. (2011). HIV infection, inflammation, immunosenescence, and aging. Annu. Rev. Med. *62*, 141–155.

Deeks, S.G., Tracy, R., and Douek, D.C. (2013). Systemic effects of inflammation on health during chronic HIV infection. Immunity *39*, 633–645.

Derr, A., Yang, C., Zilionis, R., Sergushichev, A., Blodgett, D.M., Redick, S., Bortell, R., Luban, J., Harlan, D.M., Kadener, S., et al. (2016). End Sequence Analysis Toolkit (ESAT) expands the extractable information from single-cell RNA-seq data. Genome Res. *26*, 1397–1410.

Eberl, G., Di Santo, J.P., and Vivier, E. (2015). The brave new world of innate lymphoid cells. Nat. Immunol. *16*, 1–5.

Favre, D., Mold, J., Hunt, P.W., Kanwar, B., Loke, P. 'ng, Seu, L., Barbour, J.D., Lowe, M.M., Jayawardene, A., Aweeka, F., et al. (2010). Tryptophan catabolism by indoleamine 2,3-dioxygenase 1 alters the balance of TH17 to regulatory T cells in HIV disease. Sci. Transl. Med. *2*, 32ra36.

Freiberg, M.S., Chang, C.-C.H., Kuller, L.H., Skanderson, M., Lowy, E., Kraemer, K.L., Butt, A.A., Bidwell Goetz, M., Leaf, D., Oursler, K.A., et al. (2013). HIV infection and the risk of acute myocardial infarction. JAMA Intern. Med. *173*, 614–622.

Gordon, S.M., Chaix, J., Rupp, L.J., Wu, J., Madera, S., Sun, J.C., Lindsten, T., and Reiner, S.L. (2012). The transcription factors T-bet and Eomes control key checkpoints of natural killer cell maturation. Immunity *36*, 55–67.

Günthard, H.F., Saag, M.S., Benson, C.A., del Rio, C., Eron, J.J., Gallant, J.E., Hoy, J.F., Mugavero, M.J., Sax, P.E., Thompson, M.A., et al. (2016). Antiretroviral Drugs for Treatment and Prevention of HIV Infection in Adults: 2016 Recommendations of the International Antiviral Society-USA Panel. JAMA *316*, 191–210.

Hashimshony, T., Senderovich, N., Avital, G., Klochendler, A., de Leeuw, Y., Anavy, L., Gennert, D., Li, S., Livak, K.J., Rozenblatt-Rosen, O., et al. (2016). CEL-Seq2: sensitive highly-multiplexed single-cell RNA-Seq. Genome Biol. *17*, 77.

Hazenberg, M.D., and Spits, H. (2014). Human innate lymphoid cells. Blood *124*, 700–709.

Hechenbichler, K., and Schliep, K. (2004). Weighted k-Nearest-Neighbor Techniques and Ordinal Classification. *399*.

Hyvärinen, A., and Oja, E. (2000). Independent component analysis: algorithms and applications. Neural Netw. *13*, 411–430.

Ishizuka, I.E., Chea, S., Gudjonson, H., Constantinides, M.G., Dinner, A.R., Bendelac, A., and Golub, R. (2016). Single-cell analysis defines the divergence between the innate lymphoid cell lineage and lymphoid tissue-inducer cell lineage. Nat. Immunol. *17*, 269–276.

Kacani, L., Stoiber, H., and Dierich, M.P. (1997). Role of IL-15 in HIV-1-associated hypergammaglobulinaemia. Clinical & Experimental Immunology *108*, 14–18.

Kim, D., Pertea, G., Trapnell, C., Pimentel, H., Kelley, R., and Salzberg, S.L. (2013). TopHat2: accurate alignment of transcriptomes in the presence of insertions, deletions and gene fusions. Genome Biol. *14*, R36.

Klatt, N.R., Estes, J.D., Sun, X., Ortiz, A.M., Barber, J.S., Harris, L.D., Cervasi, B., Yokomizo, L.K., Pan, L., Vinton, C.L., et al. (2012). Loss of mucosal CD103+ DCs and IL-17+ and IL-22+ lymphocytes is associated with mucosal damage in SIV infection. Mucosal Immunol. *5*, 646–657.

Klein, A.M., Mazutis, L., Akartuna, I., Tallapragada, N., Veres, A., Li, V., Peshkin, L., Weitz, D.A., and Kirschner, M.W. (2015). Droplet barcoding for single-cell transcriptomics applied to embryonic stem cells. Cell *161*, 1187–1201.

Klose, C.S.N., and Artis, D. (2016). Innate lymphoid cells as regulators of immunity, inflammation and tissue homeostasis. Nat. Immunol. *17*, 765–774.

Klose, C.S.N., Flach, M., Möhle, L., Rogell, L., Hoyler, T., Ebert, K., Fabiunke, C., Pfeifer, D., Sexl, V., Fonseca-Pereira, D., et al. (2014). Differentiation of type 1 ILCs from a common progenitor to all helper-like innate lymphoid cell lineages. Cell *157*, 340–356.

Kløverpris, H.N., Kazer, S.W., Mjösberg, J., Mabuka, J.M., Wellmann, A., Ndhlovu, Z., Yadon, M.C., Nhamoyebonde, S., Muenchhoff, M., Simoni, Y., et al. (2016). Innate Lymphoid Cells Are Depleted Irreversibly during Acute HIV-1 Infection in the Absence of Viral Suppression. Immunity *44*, 391–405.

Lee, J., Zhang, T., Hwang, I., Kim, A., Nitschke, L., Kim, M., Scott, J.M., Kamimura, Y., Lanier, L.L., and Kim, S. (2015). Epigenetic modification and antibody-dependent expansion of memory-like NK cells in human cytomegalovirus-infected individuals. Immunity *42*, 431–442.

Leonard, W.J., and O'Shea, J.J. (1998). Jaks and STATs: biological implications. Annu. Rev. Immunol. *16*, 293–322.

Lim, A.I., Menegatti, S., Bustamante, J., Le Bourhis, L., Allez, M., Rogge, L., Casanova, J.-L., Yssel, H., and Di Santo, J.P. (2016). IL-12 drives functional plasticity of human group 2 innate lymphoid cells. J. Exp. Med. *213*, 569–583.

Lim, A.I., Li, Y., Lopez-Lastra, S., Stadhouders, R., Paul, F., Casrouge, A., Serafini, N., Puel, A., Bustamante, J., Surace, L., et al. (2017). Systemic Human ILC Precursors

Provide a Substrate for Tissue ILC Differentiation. Cell *168*, 1086–1100.e10.

Lin, W.-H.W., Nish, S.A., Yen, B., Chen, Y.-H., Adams, W.C., Kratchmarov, R., Rothman, N.J., Bhandoola, A., Xue, H.-H., and Reiner, S.L. (2016a). CD8(+) T Lymphocyte Self-Renewal during Effector Cell Determination. Cell Rep. *17*, 1773–1782.

Lin, Z., Kuroki, K., Kuse, N., Sun, X., Akahoshi, T., Qi, Y., Chikata, T., Naruto, T., Koyanagi, M., Murakoshi, H., et al. (2016b). HIV-1 Control by NK Cells via Reduced Interaction between KIR2DL2 and HLA-C(∗)12:02/C(∗)14:03. Cell Rep. *17*, 2210–2220.

Liu, J., Pan, S., Hsieh, M.H., Ng, N., Sun, F., Wang, T., Kasibhatla, S., Schuller, A.G., Li, A.G., Cheng, D., et al. (2013). Targeting Wnt-driven cancer through the inhibition of Porcupine by LGK974. Proc. Natl. Acad. Sci. U. S. A. *110*, 20224–20229.

Love, M., Anders, S., and Huber, W. (2014). Differential analysis of count data--the DESeq2 package. Genome Biol. *15*, 550.

Luther, S.A., Mark Ansel, K., and Cyster, J.G. (2003). Overlapping Roles of CXCL13, Interleukin 7 Receptor α, and CCR7 Ligands in Lymph Node Development. J. Exp. Med. *197*, 1191–1198.

Margolis, D.M., Garcia, J.V., Hazuda, D.J., and Haynes, B.F. (2016). Latency reversal and viral clearance to cure HIV-1. Science *353*, aaf6517.

Massanella, M., Gómez-Mora, E., Carrillo, J., Curriu, M., Ouchi, D., Puig, J., Negredo, E., Cabrera, C., Clotet, B., and Blanco, J. (2015). Increased ex vivo cell death of central memory CD4 T cells in treated HIV infected individuals with unsatisfactory immune recovery. J. Transl. Med. *13*, 230.

Moretta, L. (2010). Dissecting CD56dim human NK cells. Blood *116*, 3689–3691.

Mortha, A., Chudnovskiy, A., Hashimoto, D., Bogunovic, M., Spencer, S.P., Belkaid, Y., and Merad, M. (2014). Microbiota-dependent crosstalk between macrophages and ILC3 promotes intestinal homeostasis. Science *343*, 1249288.

Neri, S., Mariani, E., Meneghetti, A., Cattini, L., and Facchini, A. (2001). Calcein-acetyoxymethyl cytotoxicity assay: standardization of a method allowing additional analyses on recovered effector cells and supernatants. Clin. Diagn. Lab. Immunol. *8*, 1131–1135.

Nusse, R., and Clevers, H. (2017). Wnt/β-Catenin Signaling, Disease, and Emerging Therapeutic Modalities. Cell *169*, 985–999.

Paust, S., Gill, H.S., Wang, B.-Z., Flynn, M.P., Ashley Moseman, E., Senman, B., Szczepanik, M., Telenti, A., Askenase, P.W., Compans, R.W., et al. (2010). Critical role for the chemokine receptor CXCR6 in NK cell-mediated antigen-specific memory of haptens and viruses. Nat. Immunol. *11*, 1127–1135.

Poli, A., Michel, T., Thérésine, M., Andrès, E., Hentges, F., and Zimmer, J. (2009). CD56bright natural killer (NK) cells: an important NK cell subset. Immunology *126*, 458–465.

Reeves, R.K., Li, H., Jost, S., Blass, E., Li, H., Schafer, J.L., Varner, V., Manickam, C., Eslamizar, L., Altfeld, M., et al. (2015). Antigen-specific NK cell memory in rhesus macaques. Nat. Immunol. *16*, 927–932.

Roberts, L., Passmore, J.-A.S., Williamson, C., Little, F., Bebell, L.M., Mlisana, K., Burgers, W.A., van Loggerenberg, F., Walzl, G., Djoba Siawaya, J.F., et al. (2010). Plasma cytokine levels during acute HIV-1 infection predict HIV disease progression. AIDS *24*, 819–831.

Romee, R., Schneider, S.E., Leong, J.W., Chase, J.M., Keppel, C.R., Sullivan, R.P., Cooper, M.A., and Fehniger, T.A. (2012). Cytokine activation induces human memory-like NK cells. Blood *120*, 4751–4760.

Schmutz, S., Bosco, N., Chappaz, S., Boyman, O., Acha-Orbea, H., Ceredig, R., Rolink, A.G., and Finke, D. (2009). Cutting edge: IL-7 regulates the peripheral pool of adult ROR gamma+ lymphoid tissue inducer cells. J. Immunol. *183*, 2217–2221.

Serafini, N., Vosshenrich, C.A.J., and Di Santo, J.P. (2015). Transcriptional regulation of innate lymphoid cell fate. Nat. Rev. Immunol. *15*, 415–428.

Shebl, F.M., Yu, K., Landgren, O., Goedert, J.J., and Rabkin, C.S. (2012). Increased Levels of Circulating Cytokines with HIV-Related Immunosuppression. AIDS Res. Hum. Retroviruses *28*, 809–815.

Sinha, A., Ma, Y., Scherzer, R., Hur, S., Li, D., Ganz, P., Deeks, S.G., and Hsue, P.Y. (2016). Role of T-Cell Dysfunction, Inflammation, and Coagulation in Microvascular Disease in HIV. J. Am. Heart Assoc. *5*, e004243.

Spits, H., and Di Santo, J.P. (2011). The expanding family of innate lymphoid cells: regulators and effectors of immunity and tissue remodeling. Nat. Immunol. *12*, 21–27.

Spits, H., Artis, D., Colonna, M., and Diefenbach, A. (2013). Innate lymphoid cells—a proposal for uniform nomenclature. Nat. Rev.

Spits, H., Bernink, J.H., and Lanier, L. (2016). NK cells and type 1 innate lymphoid cells: partners in host defense. Nat. Immunol. *17*, 758–764.

Stacey, A.R., Norris, P.J., Qin, L., Haygreen, E.A., Taylor, E., Heitman, J., Lebedeva, M., DeCamp, A., Li, D., Grove, D., et al. (2009). Induction of a striking systemic cytokine cascade prior to peak viremia in acute human immunodeficiency virus type 1 infection, in contrast to more modest and delayed responses in acute hepatitis B and C virus infections. J. Virol. *83*, 3719–3733.

Suzuki, K., Nakajima, H., Saito, Y., Saito, T., Leonard, W.J., and Iwamoto, I. (2000).

Janus kinase 3 (Jak3) is essential for common cytokine receptor gamma chain (gamma(c))-dependent signaling: comparative analysis of gamma(c), Jak3, and gamma(c) and Jak3 double-deficient mice. Int. Immunol. *12*, 123–132.

Swaminathan, S., Qiu, J., Rupert, A.W., Hu, Z., Higgins, J., Dewar, R.L., Stevens, R., Rehm, C.A., Metcalf, J.A., Sherman, B.T., et al. (2016). Interleukin-15 (IL-15) Strongly Correlates with Increasing HIV-1 Viremia and Markers of Inflammation. PLoS One *11*, e0167091.

Taieb, F., Madec, Y., Cournil, A., and Delaporte, E. (2017). Virological success after 12 and 24 months of antiretroviral therapy in sub-Saharan Africa: Comparing results of trials, cohorts and cross-sectional studies using a systematic review and meta-analysis. PLoS One *12*, e0174767.

Tibshirani, R., and Walther, G. (2005). Cluster Validation by Prediction Strength. J. Comput. Graph. Stat. *14*, 511–528.

Trapnell, C., Cacchiarelli, D., Grimsby, J., Pokharel, P., Li, S., Morse, M., Lennon, N.J., Livak, K.J., Mikkelsen, T.S., and Rinn, J.L. (2014). The dynamics and regulators of cell fate decisions are revealed by pseudotemporal ordering of single cells. Nat. Biotechnol. *32*, 381–386.

Tucker, J.D., Tso, L.S., Hall, B., Ma, Q., Beanland, R., Best, J., Li, H., Lackey, M., Marley, G., Rich, Z.C., et al. (2017). Enhancing Public Health HIV Interventions: A Qualitative Meta-Synthesis and Systematic Review of Studies to Improve Linkage to Care, Adherence, and Retention. EBioMedicine *17*, 163–171.

Utzschneider, D.T., Charmoy, M., Chennupati, V., Pousse, L., Ferreira, D.P., Calderon-Copete, S., Danilo, M., Alfei, F., Hofmann, M., Wieland, D., et al. (2016). T Cell Factor 1-Expressing Memory-like CD8(+) T Cells Sustain the Immune Response to Chronic Viral Infections. Immunity *45*, 415–427.

Van Der Maaten, L. (2014). Accelerating t-SNE using tree-based algorithms. J. Mach. Learn. Res. *15*, 3221–3245.

Vivier, E., Tomasello, E., Baratin, M., Walzer, T., and Ugolini, S. (2008). Functions of natural killer cells. Nat. Immunol. *9*, 503–510.

Vonarbourg, C., and Diefenbach, A. (2012). Multifaceted roles of interleukin-7 signaling for the development and function of innate lymphoid cells. Semin. Immunol. *24*, 165–174.

Walker, J.A., Barlow, J.L., and McKenzie, A.N.J. (2013). Innate lymphoid cells — how did we miss them? Nat. Rev. Immunol. *13*, 75.

van de Wetering, M., Sancho, E., Verweij, C., de Lau, W., Oving, I., Hurlstone, A., van der Horn, K., Batlle, E., Coudreuse, D., Haramis, A.-P., et al. (2002). The β-Catenin/TCF-4 Complex Imposes a Crypt Progenitor Phenotype on Colorectal Cancer

Cells. Cell *111*, 241–250.

Yu, J., Wei, M., Mao, H., Zhang, J., Hughes, T., Mitsui, T., Park, I.-K., Hwang, C., Liu, S., Marcucci, G., et al. (2009). CD94 defines phenotypically and functionally distinct mouse NK cell subsets. J. Immunol. *183*, 4968–4974.

Zheng, Y., Valdez, P.A., Danilenko, D.M., Hu, Y., Sa, S.M., Gong, Q., Abbas, A.R., Modrusan, Z., Ghilardi, N., de Sauvage, F.J., et al. (2008). Interleukin-22 mediates early host defense against attaching and effacing bacterial pathogens. Nat. Med. *14*, 282–289.

FIGURE LEGENDS

Figure 1. Major Populations of TBX21$^+$ILC1s and RORγT$^+$ILC3s in Human Blood and Colon are CD127$^-$

(A, B) Flow cytometry for CD127 versus pool of 12 lineage markers after gating for viable, singlet, lymphoid PBMCs (A), and for TBX21, CRTH2, or RORγT among Lin$^-$ (B). (C, D) Percentage of TBX21$^+$ (C, n=16), or RORγT$^+$ (D, n=19), among the indicated subpopulations. (E, F) CD127 versus TBX21$^+$ or RORγT$^+$ among Lin$^-$ umbilical cord blood (E) or colon lamina propria lymphoid cells (F). (G, H) Percentage of the indicated populations from cord blood (G, n=15; H, n=16). (I, J) Percentage of the indicated populations from colon (I, n=5; J, n=6). (K, L) TBX21 versus IFN-γ, GM-CSF, or TNFα after Lin$^-$PBMCs were stimulated with PMA and ionomycin (K) or IL-12 and IL-15 (L). (M) Lin$^-$ lamina propria lymphoid cells stimulated with PMA and ionomycin and stained for CD127 versus IL-22 or IL-13. Data are representative of ≥ 3 donors. Each dot represents 1 donor, mean ± s.e.m.; two-tailed, unpaired *t*-test; ns, non-significant, $^*p<0.05$, $^{**}p<0.01$, $^{***}p<0.001$; See also Figures S1-S2.

Figure 2. CD127$^+$ILCs and CD127$^-$ILC1s are Decreased in Blood and Colon of HIV-1$^+$ People on Effective Antiviral Therapy

(A) Flow cytometry for 12 lineage markers versus CD127 on PBMCs from HIV-1$^-$ and HIV-1$^+$ individuals. (B) Percentage of CD127$^+$ cells among Lin$^-$PBMCs from HIV-1$^-$ (n=23), and HIV-1$^+$ (n=28). (C-E) Lin$^-$PBMCs from HIV-1$^-$ or HIV-1$^+$ were analyzed by flow cytometry with CD127 and either TBX21 (C), CRTH2 (D) or RORγT (E). (F-H) Percentage of TBX21$^+$ (F), HIV-1$^-$ (n=14), HIV-1$^+$ (n=22); CRTH2$^+$ (G), HIV-1$^-$ (n=9), HIV-1$^+$ (n=10); or RORγT$^+$ (H), HIV-1$^-$ (n=14), HIV-1$^+$ (n=21), from (C-E). (I) Human lamina propria lymphocytes were detected with 12 lineage markers and CD127 (left), and Lin$^-$ cells were further analyzed with CD127 and RORγT (right). (J, K) Percentage of Lin$^-$CD127$^+$ (J), HIV-1$^-$ (n=6), HIV-1$^+$ (n=7), or Lin$^-$RORγT$^+$CD127$^+$ (K), HIV-1$^-$ (n=6), HIV-1$^+$ (n=7). (L) Lamina propria CD127$^+$ILC3s maintain the integrity of gut epithelium by producing cytokines such as IL-22 (left). HIV-1 infection is associated with irreversible elimination of CD127$^+$ILCs and disrupted intestinal epithelium (right). Each

dot represents a unique sample, mean ± s.e.m.; two-tailed unpaired *t*-test; ns, non-significant, $^{***}p<0.001$. See also Figure S3.

Figure 3. HIV-1 Shifts the Balance from CD127^{+}ILCs to CD127^{-}ILCs

(A, B) PBMCs were stimulated with PMA and ionomycin, or with the indicated cytokines for 16 hrs. The CD127^{+}ILC percentage among Lin^{-}TBX21^{-} cells was determined by flow cytometry (A) and calculated (n=3) (B). (C) The percentage CD127^{+}ILCs among Lin^{-} PBMCs was calculated after treatment with the indicated common γ chain cytokines for 16 hs (n=4). (D) IL-7 treatment shifted CD127^{+}ILCs to CD127^{-}ILCs; CD25 and CD127 were detected on Lin^{-} PBMC, with or without IL-7 treatment. (E) PBMCs were treated with IL-7 or IL-15 for 16 hrs, with or without JAK1/2 inhibitor Ruxolitinib, or JAK3 inhibitor CP-690550, and the percentage CD127^{+}ILCs among Lin^{-} cells was calculated (n=4). mean ± s.e.m., two-tailed unpaired *t*-test, $^{**}p<0.01$, $^{***}p<0.001$. See also Figure S4.

Figure 4. HIV-1 Shifts the Balance from CD127^{-}ILC1s to NK Cells

(A, B) PBMCs from HIV-1^{-} and HIV-1^{+} people were stained with lineage markers, but leaving out the anti-CD94 antibody (*Lin), and then the percent CD94^{-} and CD94^{+} among the *Lin^{-}TBX21^{+} population was determined (A), CD94^{+}/CD94^{-} ratio (B), HIV-1^{-} (n=23), HIV-1^{+} (n=26). (C, D) Percent CD94^{-} and CD94^{+} among *Lin^{-}TBX21^{+}PBMCs after stimulation with PMA and ionomycin or IL-15 (C), CD94^{-}/CD94^{+} ratio (D) (n=10). (E-G) CD127^{-}ILC1s were sorted as *Lin^{-}CD56^{+}CD94^{-}, then stimulated with PMA/iono (E and F) or IL-12 + IL-15 (G) for 16 hrs, and the percent CD94^{+} was determined (F, n=5; G, n=6). (H) PBMCs were stimulated with PMA/iono and the percentage CD107a^{+} cells among CD127^{-}ILC1s and NK cells was calculated (n=5). (I) Percent specific lysis of K562 or Jurkat cells by sorted CD127^{-}ILC1s (*Lin^{-}CD56^{+}CD94^{-}) and NK cells (*Lin^{-} CD56^{+}CD94^{+}) (n=8). (J) Heatmap of differentially expressed genes by bulk RNA-Seq comparing CD127^{-}ILC1s and CD94^{+}NK cells, sorted from two donors. (K) Flow cytometry analysis of proteins encoded by the indicated genes from bulk RNA-seq from at least 3 independent experiments. Each dot represents a unique sample, mean ± s.e.m.; (D, H, and I), lines connect cells from common donor. (B, F and G), two-tailed

unpaired *t*-test. (D, H, and I), two-tailed paired *t*-test; $^{*}p<0.05$, $^{**}p<0.01$, $^{***}p<0.001$. See also Figures S4 and S5.

Figure 5. CD127^{-}ILC1s Act as Precursors of TCF7^{+}NK Cells

(A, B) Two dimensional (tSNE) plot of 986 CD127^{-}ILC1s and 767 CD94^{+}NK cells, color-coded according to CD127^{-}ILC1s or CD94^{+}NK cells (A), or total cells segregated into two clusters based on spectral clustering of single cell transcriptomes, with k-nearest neighbor, search=2 (B). (C) Heatmap of 1,729 CD127^{-}ILC1s (blue) and 1,548 NK cells (yellow) collected from 2 donors using all differentially expressed genes from the spectral cluster analysis. (D) Minimum spanning tree based on the transcriptome of individual cells showing the pseudotime trajectory (black line). (E) TCF7 expression profile along the pseudotime trajectory. (F) Expression level and density of the indicated genes within t-SNE plots. (A, B, D, E, and F) data are representative of two donors. (G) Sorted CD127^{-}ILC1s (*Lin^{-}CD56^{+}CD94^{-}) were treated with IL-15 (5 ng/ml) for 5 days then stimulated with IL-12 (50 ng/ml) and IL-15 (50 ng/ml) for 16 hrs. TCF7, CXCR3, CXCR6, CD44, and GZMK were detected by flow cytometry. Unstimulated CD127^{-} ILC1s from the same donor were used for the control. For TCF7 detection, data are representative of 8 donors; for CXCR3, CXCR6, CD44 and GZMK, data are representative of 4 donors. *Lin denotes the panel of lineage marker antibodies that does not include anti-CD94. See also Figure S6 and S7.

Figure 6. WNT Inhibition Blocks the Cytokine Induced Transition of CD127^{-}ILC1 into NK Memory Cells

(A-D) PBMCs (A and B) or sorted CD127^{-}ILC1s (C and D) were stimulated (Stim) with IL-12 (50 ng/ml) and IL-15 (50 ng/ml) for 16 hrs, or not stimulated (NS), in the presence of LGK974 (10 uM), as indicated. CD94 levels on the *Lin^{-}TBX21^{+} population were detected (A) and the ratio of CD94^{+}/CD94^{-} was calculated (B) (NS, n=22; Stim n=26; Stim+LGK974, n=26); The percent of CD94 was also detected (C) and calculated (D) (n=15) for sorted CD127^{-}ILC1s. (E and F) PBMCs were stimulated with IL-15 (50 ng/ml) for 5 days, with or without LGK974 (10 uM). The *Lin^{-}CD56^{+} population was assessed for CD56 and CD94 (E), and the percentage of CD56^{hi} among *Lin^{-}CD56^{+} cells was

calculated (F) (n=10). (G and H) PBMCs incubated in the presence or absence of LGK974 (10 uM) were treated for 16 hrs (Pre-stim) with IL-12 (10 ng/ml), IL-15 (5 ng/ml), and IL-18 (50 ng/ml), or not (No pre-stim), and incubated for 5 days in IL-15 (5 ng/ml). All cells were then stimulated with IL-12 (50 ng/ml) and IL-15 (50 ng/ml) for 16 hrs, and cell associated IFN-γ and CD94 were detected in the *Lin$^-$TBX21$^+$ population (G), and the result was calculated (H) (n=13). Each dot represents a unique donor, mean ± s.e.m.; (B, D, F and H), two-tailed paired *t*-test. $^{***}p<0.001$. *Lin denotes the panel of lineage marker antibodies that does not include anti-CD94. See also Figures S7.

Figure 7. HIV-1 Infection Increases TCF7$^+$NK Cells

(A and B) TCF7 in CD127$^-$ILC1s and CD94$^+$NK cells was detected (A) and calculated (B) in PBMCs from HIV-1$^-$ (n=21) and HIV-1$^+$ (n=11) individuals. (C and D) The *Lin$^-$TBX21$^+$ population from PBMCs of HIV-1$^-$ (n=9) and HIV-1$^+$ (n=10) people was detected with NKG2C (C) and results were calculated (D). (E) Model for plasticity of CD127$^-$ILC1s. Among ILC1s, the vast majority are CD127$^-$ (left). Inflammation associated with HIV-1 infection unmasks CD127$^-$ILC1 plasticity (right), generating increased percentages of CD94$^+$effector and TCF7$^+$memory NK cells. Upon immune stimulation, memory NK cells also give rise to effector NK cells. Two-tailed unpaired *t*-test; mean ± s.e.m.; $^{**}p<0.01$, $^{***}p<0.001$. *Lin denotes the panel of lineage marker antibodies that does not include anti-CD94.

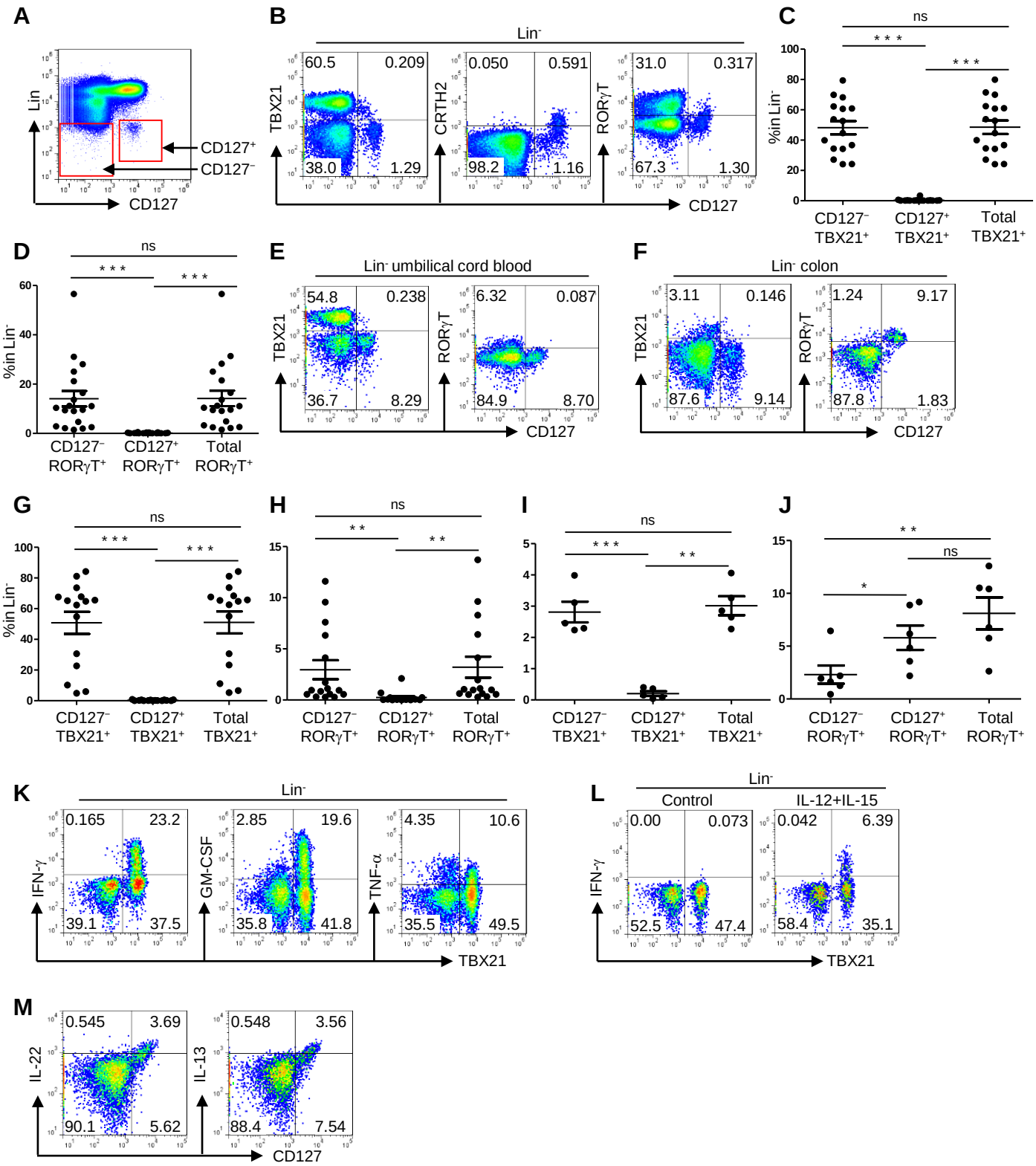

Wang et al, Figure 1

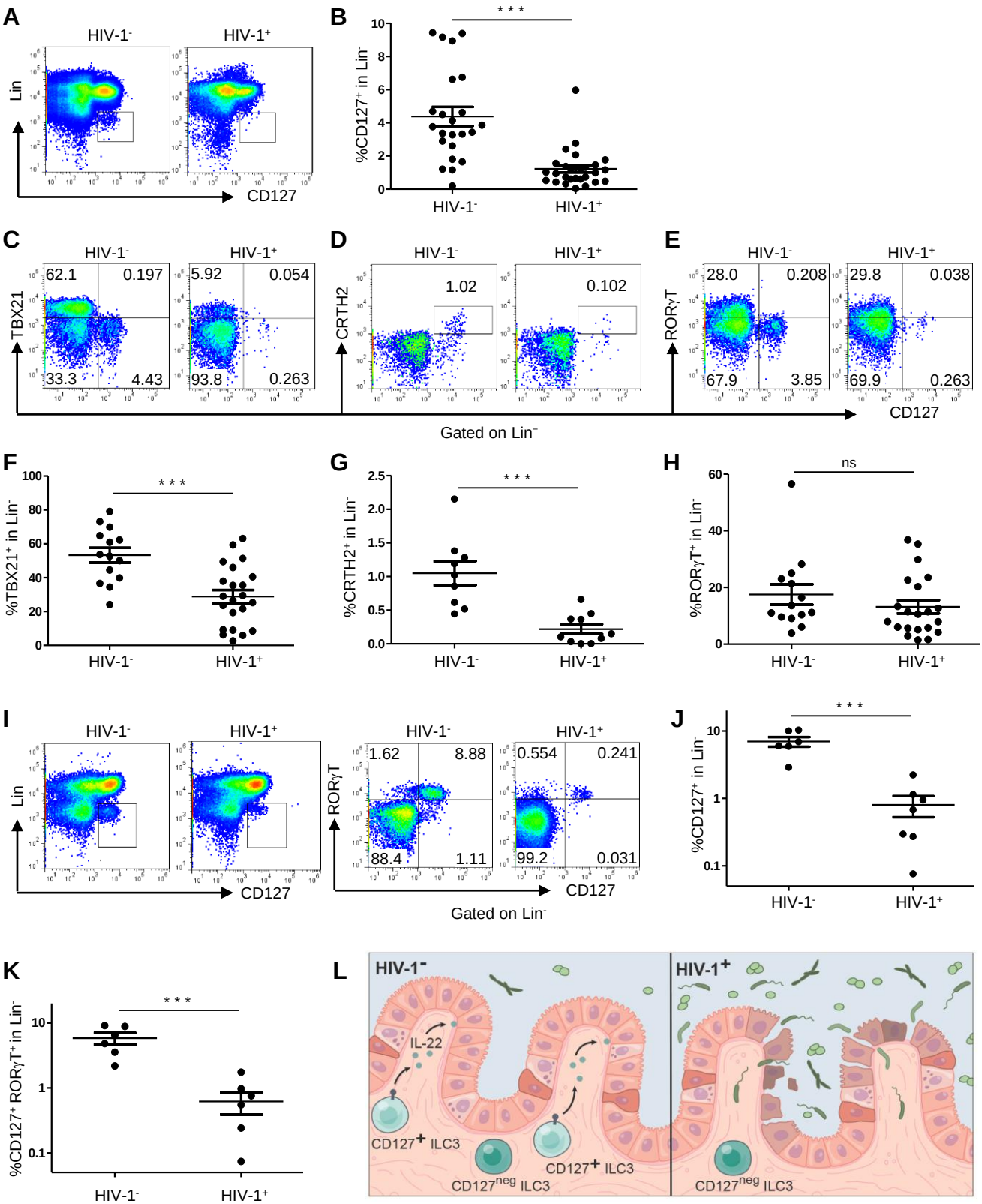

Wang et al, Figure 2

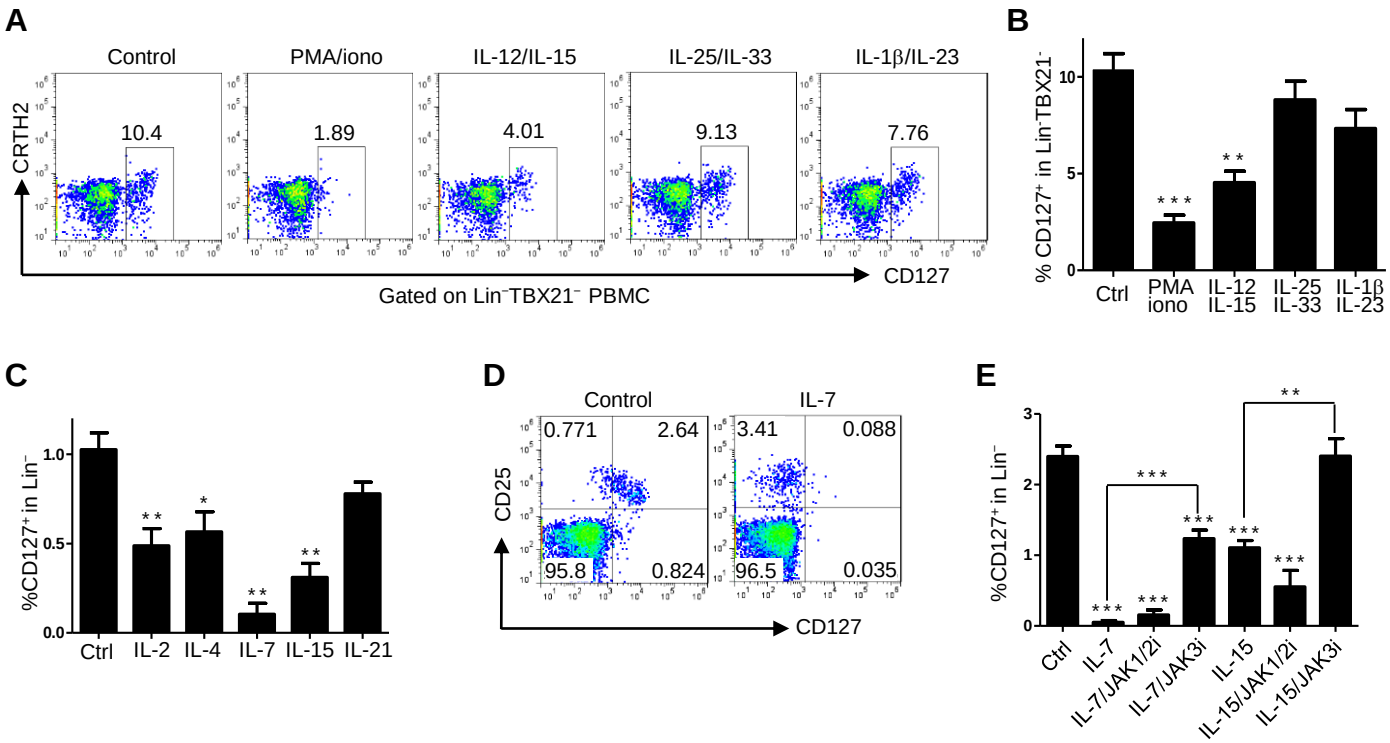

Wang et al, Figure 3

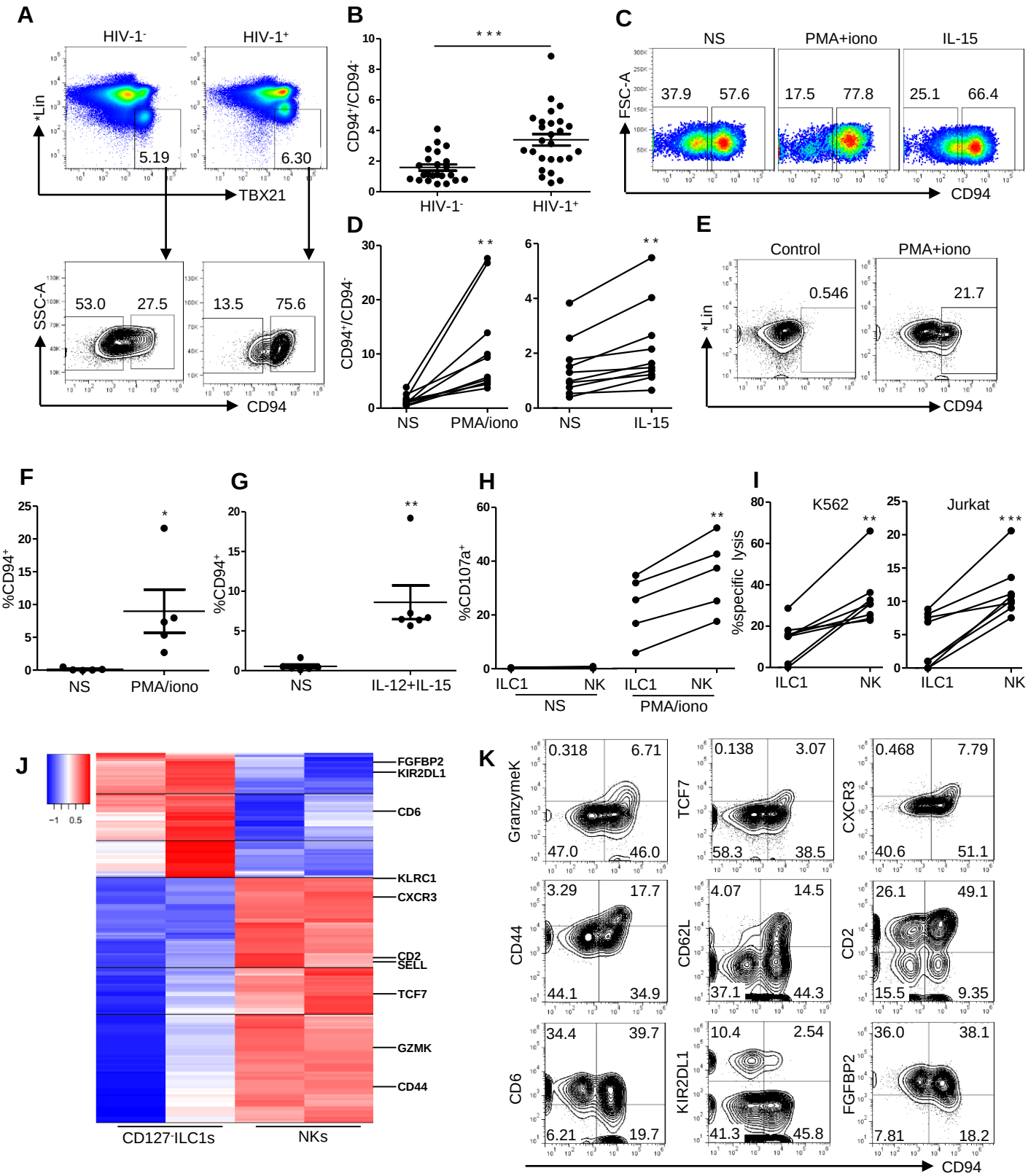

Wang et al, Figure 4

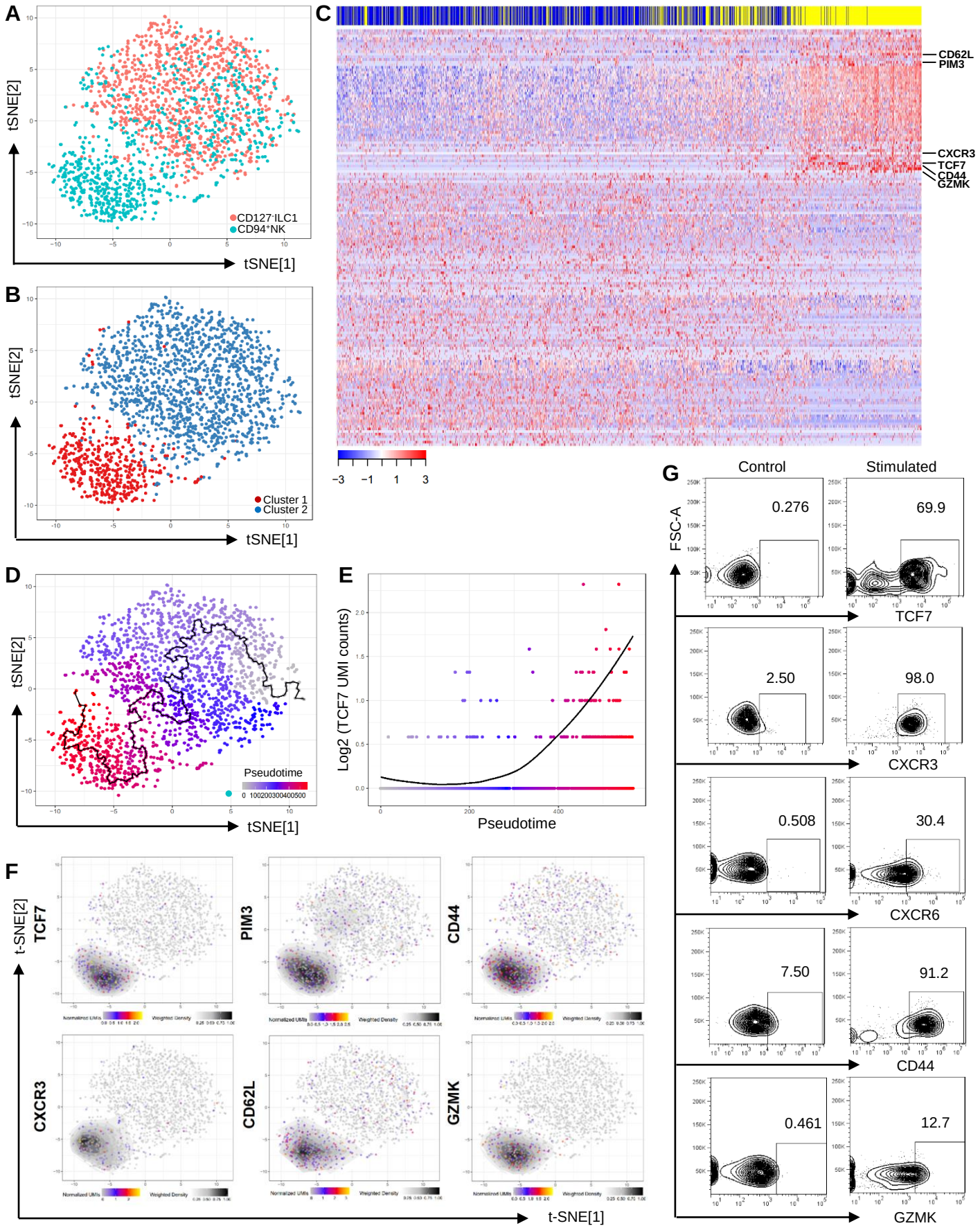

Wang et al, Figure 5

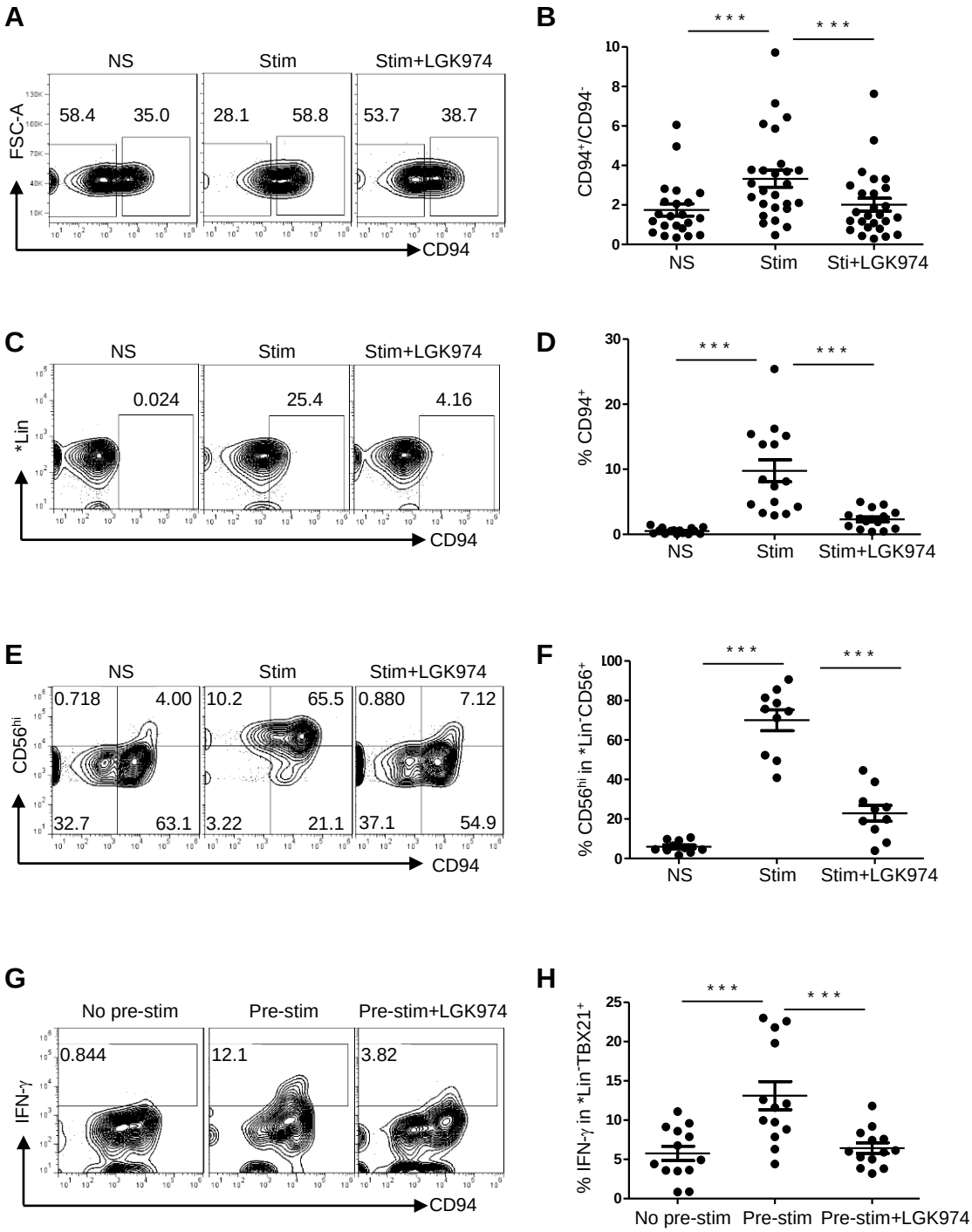

Wang et al, Figure 6

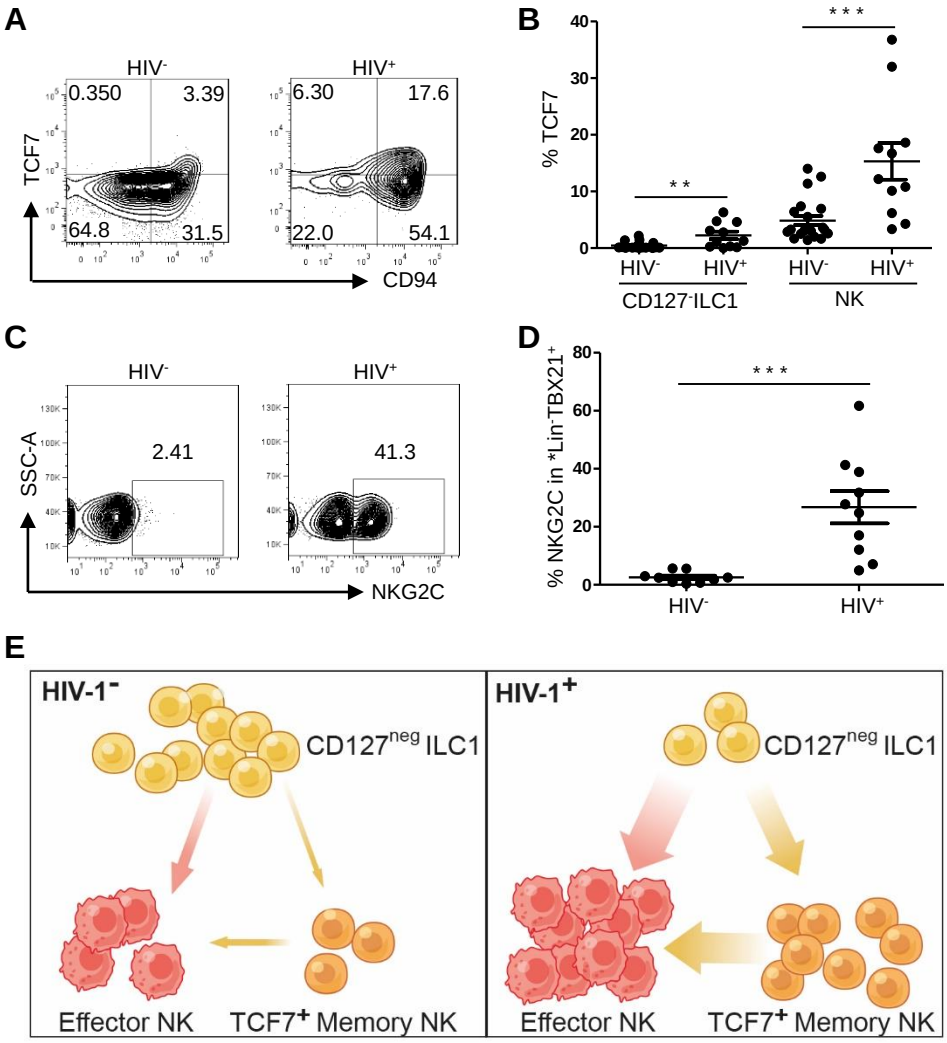

Wang et al, Figure 7